THE EFFECTS OF CHALCOPYRITE TRACE ELEMENTS ON RESISTIVITY

by

Sarah Patterson

A Thesis Submitted to the Faculty of the

SCHOOL OF MINING ENGINEERING AND MINERAL RESOURCES

In Partial Fulfillment of the Requirements

For the Degree of

MASTER OF SCIENCE

In the Graduate College

THE UNIVERSITY OF ARIZONA

2025

THE UNIVERSITY OF ARIZONA
GRADUATE COLLEGE

As members of the Master's Committee, we certify that we have read the thesis prepared by: Sarah Nicole Patterson,
titled: The Effects of Chalcopyrite Trace Elements on Resistivity

and recommend that it be accepted as fulfilling the thesis requirement for the Master's Degree.

Isabel Barton ______________________ Date: 8/21/25
Committee Chair: *Dr. Isabel Barton*

______________________ Date: 8/21/25
Dr. Andrew Wessman

______________________ Date: 8/21/25
Dr. Selo Ndlovu

Isabel Barton ______________________ Date: 8/21/25
Dr. Isabel Barton

Final approval and acceptance of this thesis is contingent upon the candidate's submission of the final copies of the thesis to the Graduate College.

I hereby certify that I have read this thesis prepared under my direction and recommend that it be accepted as fulfilling the Master's requirement.

Isabel Barton ______________________ Date: 8/21/25
Dr. Isabel Barton
Master's Thesis Committee Chair
School of Mining Engineering and Mineral Resources

Acknowledgements

This project is supported by Freeport McMoRan, most notably by Mitchell Catling , Joanna (Jodie) Robertson, and Vaibhav (VK) Srivastava who gave invaluable guidance and comments. A huge thank you to Jack Kieley and Julian Battaglia who have polished many samples and taken many resistivity points! And last but very much not least, thank you to Isabel Barton, Selo Ndlovu, Andrew Wessman, and Dean Riley.

Dedication

To my parents, who fed my boundless curiosity. To Eddy, for putting up with my boundless curiosity. To Heather and my friends, who keep me sane. And to myself, because finishing the first is always the hardest.

Table of Contents

1.0 Abstract

This paper presents preliminary data toward resolving some of the wild inconsistencies observed in the leaching behavior of chalcopyrite ($CuFeS_2$), a common copper ore mineral notorious for variable but generally poor recovery in hydrometallurgy. Ongoing research has found major inconsistencies in activation energy, dissolution mechanisms, and other leaching phenomena, even for chalcopyrites leached in the same solution. One current hypothesis for this variability is the semiconducting properties of chalcopyrite, which are thought to vary as a function of their composition. Crystallographic defects, impurities such as Zn, Ag, Ni, and Se, and major-element ratios are all thought to influence the semiconducting properties of chalcopyrite, like charge carrier type, density, and resistivity, thus accelerating or restricting dissolution. If the true determinant of these properties in natural chalcopyrite is better known, then industry can increase recovery by tailored processing strategies. However, the literature contains few measurements of semiconducting properties for natural samples, and even fewer correlated with sample composition.

In this research, the trace element compositions of 14 high-grade natural chalcopyrite samples from several deposit types are measured for resistivity. Results suggest that individual trace elements have little to do with the resistivity of chalcopyrite. The highest correlations are with Co, Ga, Ag, and Se, but top out at $R^2 = 0.45$ (Co). Modest correlations also emerge when the trace elements are grouped by substitution of crystallographic site. The strongest correlations are with the combined substitution of As, Se, and Te into the S site ($0.3 < R^2 < 0.4$). While experiments to understand the connections between sulfur deficiency, trace element substitution, and leaching have not been done, tentative conclusions from sulfur-deficient (Cu-oversaturated) chalcopyrite samples show an increase in dissolution rate.

These preliminary results suggest that the semiconducting properties of chalcopyrite emerge from a complex mix of factors, including deposit type, and are only partly related to trace element composition. They also indicate the potential limitations of attempts to understand chalcopyrite leaching phenomena with single-element approaches. Further work will focus on testing more chalcopyrite samples from constrained deposit types to improve the consistency of data.

2.0 Introduction

2.1 Background and problem statement

Chalcopyrite ($CuFeS_2$) is a common ore mineral in porphyry copper deposits, which produce roughly 70% of the world's extracted copper (Singer, 2017). Chalcopyrite is primarily treated through pyrometallurgy, which requires comminution, flotation, and concentrate shipment before smelting to separate copper. The power, heat, and water requirements make pyrometallurgy an expensive process. In contrast, leaching or hydrometallurgy uses sulfuric acid with Fe^{3+} and other dissolved ions to oxidize the Cu^+ ions from the chalcopyrite lattice into solution. This requires comparatively minimal processing, making it more economic and environmentally friendly. However, the most amenable minerals to heap leaching are copper oxides (Dreier, 2020), and copper recovery for leaching sulfides ranges from 7-25% in ferric sulfate (Barton and Hiskey, 2022a). Increases in temperature and exotic oxidants or lixiviants can increase leaching rates and recoveries from sulfides, but are expensive and currently unfeasible for industrial application (Barton and Hiskey, 2022a).

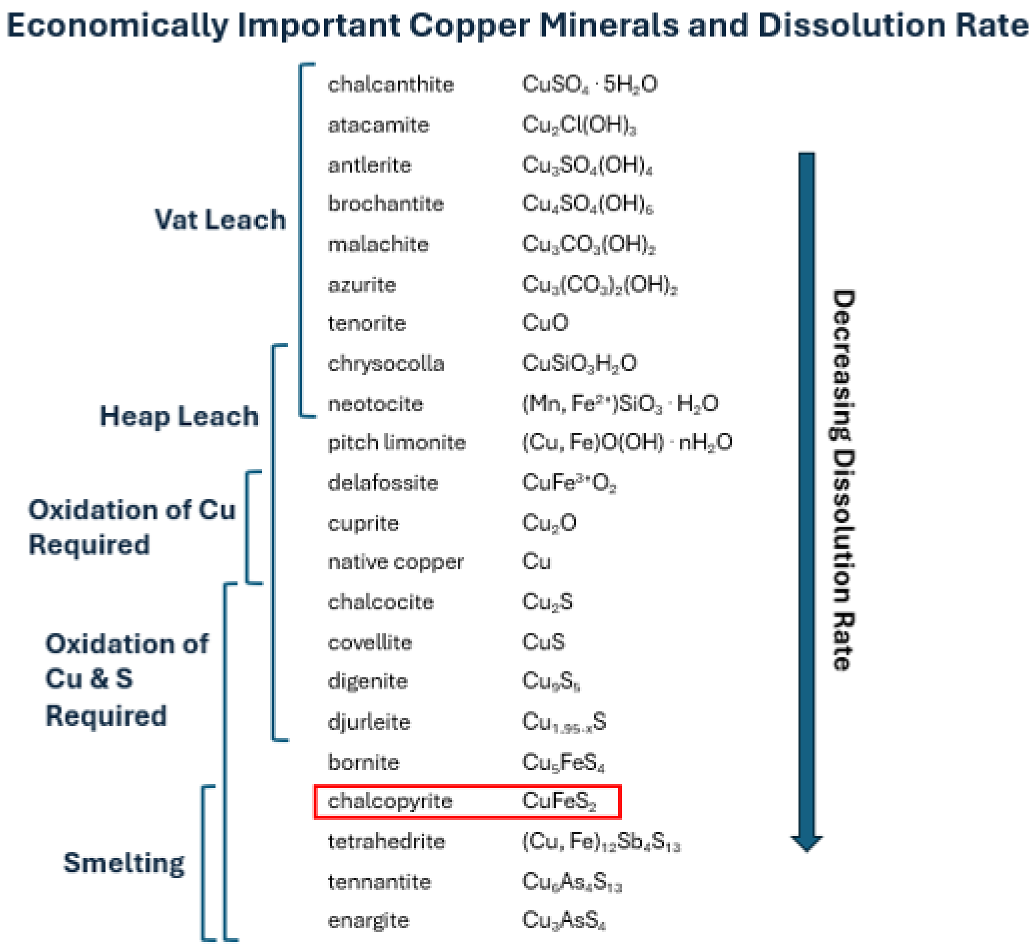

Figure 1 List of economically important copper minerals and dissolution rates, showing poor leachability of chalcopyrite. Figure from Freeport McMoran: *Introduction to Hydrometallurgy*, 2023, modified after Dreier, 2020.

The causes of the low and variable recovery from chalcopyrite leaching are poorly understood. Current hypotheses suggest:

- that a passivating surface layer forms early in leaching, inhibiting further dissolution to an unclear extent;
- that galvanic coupling of non-chalcopyrite sulfides within the ore prevent or enhance oxidation and dissolution;
- that the variable leaching results relate to the equally variable semiconducting properties of chalcopyrites from different geological settings, with different trace-element compositions.

Each of these hypotheses is complicated by further inconsistencies in the observations made to support or refute it. The formation of surface layers in some leaching systems is generally agreed upon, but their nature is not: sulfur, disulfide, polysulfide, and Fe hydroxy-oxide have all been proposed (Y. Li et al., 2013). There are also controversies over the extent to which the species observed on the surface of partially leached chalcopyrite actually cause passivation (O'Connor & Eksteen, 2020). Galvanic coupling has been observed between chalcopyrite and other sulfides within ore samples such as bornite (Cu_5FeS_4), pyrite (FeS_2), chalcocite (Cu_2S), covellite (CuS), sphalerite (ZnS), galena (PbS), and other metallic sulfides (Abraitis et al., 2004; Dutrizac, 1981; Dutrizac and MacDonald, 1973; Eghbalnia, 2012; J. Li et al., 2013; Majuste et al., 2012). However, there is no agreement on its effects; for example, some papers state that pyrite accelerates chalcopyrite leaching by a factor of 18, whereas others find no detectable increase (Abraitis et al., 2004; Nicol, 2022; Tanne & Schippers, 2021).

Compared to passivation and galvanic coupling, the last possibility – that chalcopyrite's variable leaching results relate to variation in its semiconducting properties, as determined by its trace-element composition – remains under-explored. Chalcopyrite is a natural semiconductor (Pridmore & Shuey, 1976), and the significance of semiconducting phenomena in its leaching behavior has long been recognized (e.g. Hiskey, 1993). However, early attempts to relate the resistivity and trace-element composition of natural chalcopyrite to its leaching behavior yielded inconsistent results (Dutrizac, 1981; Dutrizac & MacDonald, 1973), and such efforts were largely abandoned.

Recently, metallurgists have refocused the potential for overlap between the passivation and semiconducting hypotheses. In contrast to Dutrizac's earlier work on resistivity, the key factor in this mixed model is semiconductor type. Exact concepts vary, but generally include a depletion region either on the chalcopyrite itself or formed at the junction with the passivating layer; this depletion region prevents further electron transport and thus ends dissolution (Crundwell, 2013; Parker et al., 1981; Ren et al., 2022). Semiconductors are p-type or n-type, a designation that refers to the availability of electrons and their method of travel through the material. When a semiconductor – in this case, $CuFeS_2$ – has more electrons than stoichiometrically ideal, it is considered n-type; p-type semiconductors have fewer electrons, creating charge 'holes' or a theoretical positive charge signifying the absence of the electrons that should be present. Trace elements that have more or fewer electrons than the major element they substitute for (dopants, in materials science), strongly influence semiconductor type.

It would take a large amount of research to resolve whether passivation, galvanic coupling, or variable semiconducting properties – or a combination thereof – explains poor and variable chalcopyrite leaching results. At the moment, the main problem standing in the way of this is poor characterization (Barton & Hiskey, 2022b). Most leaching tests in the literature use chalcopyrite concentrate, which typically ranges from 75-93% purity, or specimens whose purity is highly varied. These samples usually contain numerous, not always identified, additional sulfides also recovered during the froth flotation process and/or mixed with the chalcopyrite on the microscale. Thus, a predominant number of flask tests and electrochemical cell leach experiments on "chalcopyrite" are on mineralogically inconclusive material, inhibiting comparison between studies or an understanding of the reasons behind variable behavior. Even the metallurgical experiment that did measure trace elements and resistivity, like McMillan et al., (1982), only tested ppm values for one element (Ag) and samples contained up to 8% pyrite and silicates, which were not constrained against interference.

Thus, to compare chalcopyrite experiments, all relevant facets of chalcopyrite must be included: composition, suite of accompanying sulfides, and semiconducting properties, as described below.

2.2 Properties of natural chalcopyrite and related minerals

Mineralogically, chalcopyrite is the tetragonal arrangement of Fe^{+3}, Cu^{+1}, S^{-2} ions in a 1:1:2 ratio that doubles the zincblende structure along the c-axis. Its bonding has a mixed ionic-covalent character with both Cu and Fe, with magnetic characteristics primarily determined by the spin states of the Fe^{+3} ion. These are opposed throughout the lattice, making chalcopyrite an antiferromagnetic semiconductor (Y. Li et al., 2013). The Cu^{+} ions fill half the tetrahedral sites, the Fe^{3+} ions one-quarter of the octahedral sites. Both these sites and the interstices between sites can accommodate additional metallic and semimetal cations. This, plus variable lattice disordering and anionic substitution in the S site, is responsible for chalcopyrite's wide range of compositions and for a number of derivative Cu-Fe-S minerals, which often occur with chalcopyrite and are difficult to distinguish from it by visual or X-ray diffraction (XRD) technology (Frenzel & Frisch, 2022). Intermediate solid solution (iss) or cubic-chalcopyrite, also has the Cu:Fe:S ratio 1:1:2, but is disordered with Cu and Fe ions evenly distributed between tetrahedral and octahedral sites. The metal-stuffed derivative talnakhite (tal) has a 18:16:32 ratio ($Cu_{1.125}FeS_2$). Another close relative is isocubanite (isocub), $CuFe_2S_3$. All three are cubic. Haycockite (hay) is 4:5:8 ($CuFe_{1.2}S_2$) and orthorhombic. Mooihoekite (moo) is tetragonal like chalcopyrite, but is metal-stuffed in both sites with the ratio 9:9:16 ($Cu_{1.125}Fe_{1.125}S_2$). The majority of natural chalcopyrite samples tested have been n-type, as are all reported pure synthetic samples, but an estimated 3-5% of natural chalcopyrites are p-type (data compiled by Barton & Hiskey, 2022b; Kwon & Kim, 2025).

The trace elements substituting for Cu, Fe, and S in chalcopyrite make its behavior even more complex. The metallic ions that fit into the chalcopyrite crystal structure are shown in Figure 2, with the optimal size and charge range for substitution illustrated in red.

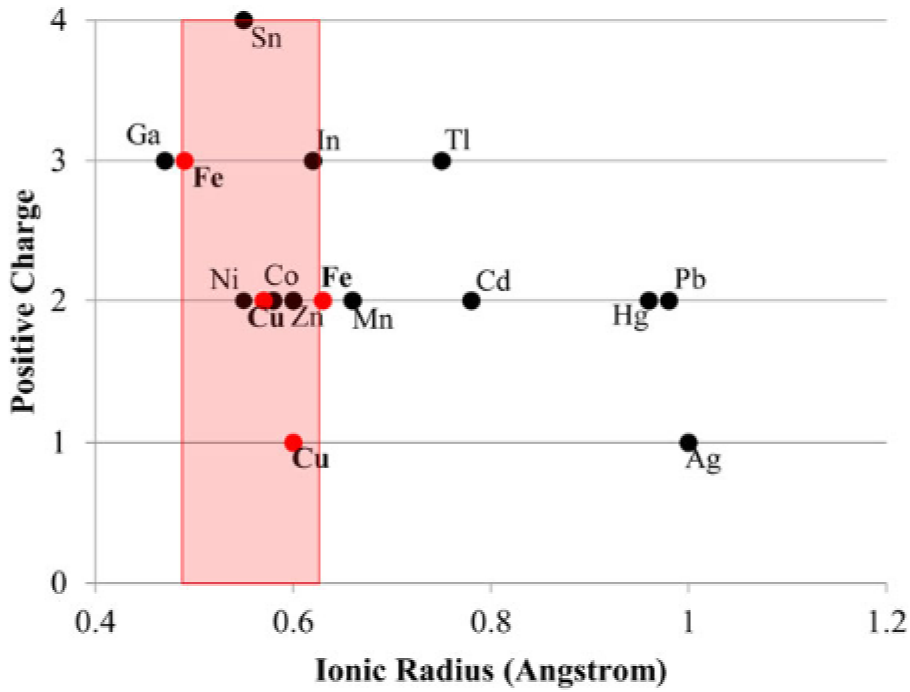

Figure 2 Plot shows the ionic radius of various trace-element ions in tetrahedral coordination. Figure after George et al., 2018.

Trace element occurrence within chalcopyrite was characterized by deposit type in a study by George et al. (2018) and are occasionally reported as part of ore genesis studies for individual deposits (Duran et al., 2017; Hawley & Nichol, 1961; Mansur et al., 2021). The results show several orders of magnitude of variation in trace-element composition between and within deposit types; for example, Zn ranges from < 0.1 - 1.8 wt% depending on the chalcopyrite and the deposit it came from (Figure 3).

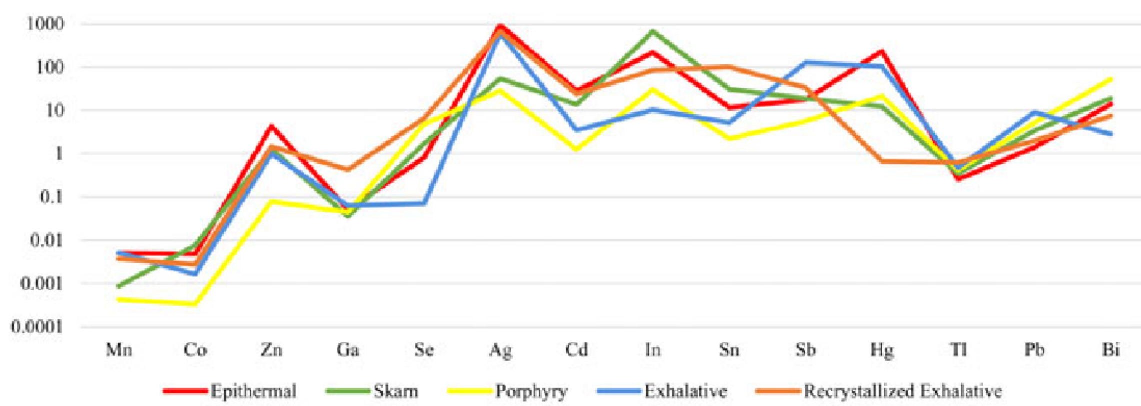

Figure 3 Comparison of the mean concentration of individual trace elements (ppm) found in chalcopyrite samples taken from different deposit types. (Figure from George et al., 2018).

These trace elements determine semiconducting properties, by increasing or decreasing conductivity via excess or deficiency in mobile electrons. Zinc in particular can influence chalcopyrite's semiconducting properties by lowering resistivity; its effects on thermal conductivity in synthetic chalcopyrite were characterized by Xie et al. (2017). Other elements investigated by George et al. (2018) have also been individually studied by materials scientists (Figure 6; Table 1), but others like Hg, Tl, Bi, and Cd, were not reported in literature and their presence may have unforeseen additional effects. Beyond that, the impact on semiconducting properties of trace elements acting in combination is almost completely unstudied. The vast majority of studies that connect chalcopyrite composition and semiconducting properties are in the materials science literature and used synthetic chalcopyrite doped with only one or two substituting elements. Natural chalcopyrites, by comparison, are extremely diverse (Figure 3).

Other than p- or n-type, resistivity is the semiconducting property thought to have the most influence on chalcopyrite leaching (e.g. Dutrizac, 1981). In the rare measurements taken on natural samples, the resistivity of chalcopyrite has been found to vary over 3-4 orders of magnitude even in samples from the same deposit types.

2.3 Current Literature

Most literature on the relevant properties of chalcopyrite focuses on its role as a semiconductor in materials science. Chalcopyrite and similar $A^{1+}B^{3+}X_2$ minerals are particularly attractive for this purpose, as they form from inexpensive, usually nontoxic, and abundant elements. They are viewed as potential replacements for current thermoelectric materials, which are composed of elements that are either rare (Te) or toxic (i.e. Bi, Pb) (Li et al., 2013). Thus, the most commonly investigated property of chalcopyrite is its thermal conductivity and power factor, which is determined by resistivity.

Pure synthetic chalcopyrite is an n-type semiconductor. Reported resistivities for it range from 0.003 Ω-cm in Teranishi and Sato (1975) to 0.15 Ω-cm in Berthebaud et al. (2015). Most accepted values rage from 0.015-0.03 Ω-cm (Tippireddy et al., 2022). In contrast to materials science literature, research into the conductivity or resistivity of natural sulfide minerals, including chalcopyrite, is minimal and rarely accompanied by trace element analysis. The first studies were conducted by Hankel (1866) and continued with Telkes (1950). Even in these early stages, both noted the orders of magnitude of variation in the resistivity of natural sulfide species. The influence of resistivity, p- or n-typing, and charge carrier mobility on leaching behavior was proposed by Gerischer (1980) and extrapolated to metallurgy by Dutrizac (1981). This was enlarged on by Parker et al. (1981), and McMillan et al. (1982a), who experimented on n- and p-type pyrite and chalcopyrite respectively. P-type chalcopyrite displayed a higher electropotential at 540 mV and 7.9 Ω-cm resistivity than n-type chalcopyrite at 500 mV and 0.12 Ω-cm. However, the n-type chalcopyrite from Timmins was only 81.9% chalcopyrite and includes 8.1% pyrite along with substantial silicates, also reported 117 ppm Ag with no other trace elements analyzed (McMillan et al., 1982b). It is uncertain but likely these inclusions affect results, considering the results from further experiments with the galvanic coupling of pyrite and chalcopyrite (Nicol, 2022).

Most materials science studies have examined the effects of specific single trace elements on chalcopyrite properties. Ge et al. (2019) replaced 10% of copper with Ag before the chalcopyrite sample showed partitioning. This sample gave a resistivity of 0.006 Ω-cm. The sample was prepared by quartz tube sintering at 960˚C for 1 day before undergoing plasma activated sintering (PAS) at 550˚C and 50 MPa for 5 minutes. Samples were analyzed via X-ray diffraction (XRD), backscatter electron microscope (BSE) and energy dispersive spectrometer (EDS), as well as a high-resolution transmission electron microscope (HRTEM).

Tippireddy et al. (2023) found that Cr^{3+} substituting in chalcopyrite is in octahedral coordination with the sulfur ions due to the exsolution of a spinel-type (Cu, Fe)Cr_3S_4 phase at even low levels of Cr substitution. The lowest chromium substitution was 2% of Cu, corresponding to a resistivity of 0.006 Ω-cm. They also found that all Cr-containing samples showed a decrease in resistivity compared to pure chalcopyrite. Synthesis used the quartz tube sintering method, then regrinding the samples and refiring them at 900˚C, before hot-pressing the powder into a pellet at 600 C and 80 Mpa for 30 minutes. Samples were identified by powder x-ray diffraction (PXRD), scanning electron microscopy (SEM), HRTEM, and EDS.

Xie et al. (2017) found that chalcopyrite with 3% of copper replaced by Zn has a resistivity of 0.007 Ω-cm, lower than the values reported for pure chalcopyrite. Experiments also showed ZnS exsolution above this concentration. However, when molar content is < 0.03, Zn substitutes for Cu and acts as an electron donor. The samples were synthesized via vacuum melting combined with the PAS process. The matrix composition of the pure chalcopyrite was identified by EDS, and when normalized to 4, forms a composition of 33.8 (S), 30.6 (Cu), and 35.5 (Fe). This actually maps to an intermediate Cu-Fe-S form between talnakhite, mooihoekite, and chalcopyrite rather than to stoichiometric chalcopyrite. However, a similar study Tsujii and Mori (2013) found a similar value for resistivity at 3% Zn in the Cu site, yielding 0.006 Ω-cm. This was lower than their measured value for pure chalcopyrite resistivity of 0.15 Ω-cm (unusually high compared to the accepted average). Their samples were sintered with the quartz tube method, heated at 700˚C for 1 day, and then maintained at 80˚C for 1 day before being ground and undergoing spark plasma sintering (SPS) at 40 MPa and 500˚C for 5 minutes. These pellets were again annealed in a silica tube with a small amount of sulfur at 350˚C added for non-stoichiometric samples. All samples were characterized by electron microprobe analysis (EPMA).

Kwon & Kim (2025) report Ni is soluble up to at least 8% substitution for Cu and yields 0.021 Ω-cm resistivity. In this study, a mechanical alloy method was used to create a sintered powder which was hot-pressed at 500˚C under 70 MPa. Identification was by XRD. While Lefèvre et al. (2016) also tested Ni, the concentrations were only at 4% substitution and corresponded to 0.01 Ω-cm resistivity. In both cases Ni appears to have minimal effect on chalcopyrite resistivity.

Lefèvre et al. (2016) tested the effects of substituting Ni, Co, Zn, and Mn while deliberately over-stuffing and under-stuffing the sulfur site. Substitution of < 8% Ni and Co for the metals yielded values corresponding to the other doping resistivities mentioned. For Mn, chalcopyrite was doped up to 4% substitution with Cu, which yielded 0.008 Ω-cm resistivity. In this study 5g samples were synthesized by the quartz tube method, heated to 800˚C for 12 hr, and then cooled over 6 hr. The obtained powders were sintered by SPS using various pressure/temperature treatments, with resulting density values found to be over >90% of theoretical. Samples were characterized by XRD at each step of synthesis as well as transmission electron microscopy (TEM), electron diffraction, (ED), and HRTEM.

Xie et al., 2016 doped chalcopyrite with up to 8% In in the Fe site and found a resistivity of 0.056 Ω-cm, higher than the typical resistivity of pure $CuFeS_2$. Samples were sintered with the quartz tube method at 1050˚C for one day and ground to powder before PAS at 550˚C and 40 MPa under vacuum. Phase structure and mineral identification were analyzed via powder XRD, field emission scanning electron microscopy (FESEM), and chemical composition with EDS. When normalized to 4 atoms, composition by weight percents was 34.0 (S), 31.0 (Fe), and 35.0 (Cu). This maps to an intermediate Cu-Fe-S form between talnakhite, mooihoekite, and chalcopyrite, so the results may not reflect the properties of stoichiometric chalcopyrite.

Teranishi and Sato (1975) reported that doping synthetic chalcopyrites with 5% Sb in the S site yielded a resistivity of 0.059 Ω-cm, higher than the resistivity of pure chalcopyrite. Doping Zn into the Fe site at levels between 5 and 10% yielded resistivities of 2.5 and 0.29 Ω-cm, while a Cu-enriched and Fe-depleted synthetic specimen had a resistivity of 0.256 Ω-cm. They used the direct melting method and identified samples via XRD. Notably, they had deliberately made all chalcopyrite samples p-types by substituting lower-valent cations and/or higher-valent anions into the metal and sulfide sites respectively.

Carr and Morelli (2016) were able to substitute up to 25% selenium for S in chalcopyrite and obtain a resistivity of 0.09 Ω-cm before doping created an exsolution of FeSe. Samples were synthesized via quartz tube sintering at 900˚C for 1 day, then slow-cooled to 300˚C for 1 day before being quenched in water. The material was placed in a ball mill for 1hr and hot-pressed into a pellet at 376˚C for 80 MPa and 15 minutes. Identification was via XRD.

Tippireddy et al. (2022) found that >4% Sn substituted for Cu exsolved a phase of isocubanite that substantially decreased the resistivities of the associated samples. At 4% Sn, resistivity was 0.006 Ω-cm. Samples were sintered via the quartz tube method and heated to 450˚C for 150hr before being cooled slowly to room temperature. Products were powdered and refired at 900˚C for 2 days, then hot-pressed at 600˚C for 30 minutes under 80 MPa. Powder XRD was used to identify the samples, along with EDS, SEM, and x-ray photoelectric spectroscopy (XPS).

Berthebaud et al. (2015) found that 8% Co substituted for Cu increased electrical resistivity to ~0.25 Ω-cm. Further experiments conducted with hot and cold-pressed pellets found that hot-pressing decreases the electrical resistivity from ~0.013 to ~0.0054 Ω-cm. This corresponds to the resistivity of Fe-rich non-stoichiometric chalcopyrite measured by Tsujii & Mori, (2013) and likely reflects sulfur loss. These samples were sintered via the quartz tube method at 600˚C for 2 days. For some compositions, the results were re-sintered by spark plasma sintering (SPS) at 50˚C at 70 MPa for 30 minutes. Samples were characterized via HRTEM and energy dispersive x-ray analysis (EDX).

These values and others for synthetic chalcopyrite relatives are summarized in Table 1 and Figure 4. It is highly likely that the disparity between "pure chalcopyrite" values are due to the range of production methods and characterization highlighted above. Despite lack of confidence in the stoichiometry of some reported "pure chalcopyrite" values, all collected literature values in Table 1 have been presented as chalcopyrite. The exception is the data from Shah et al. (2024), as their reported Cu-Fe-S wt% values are stoichiometric for mooihoekite and talnakhite.

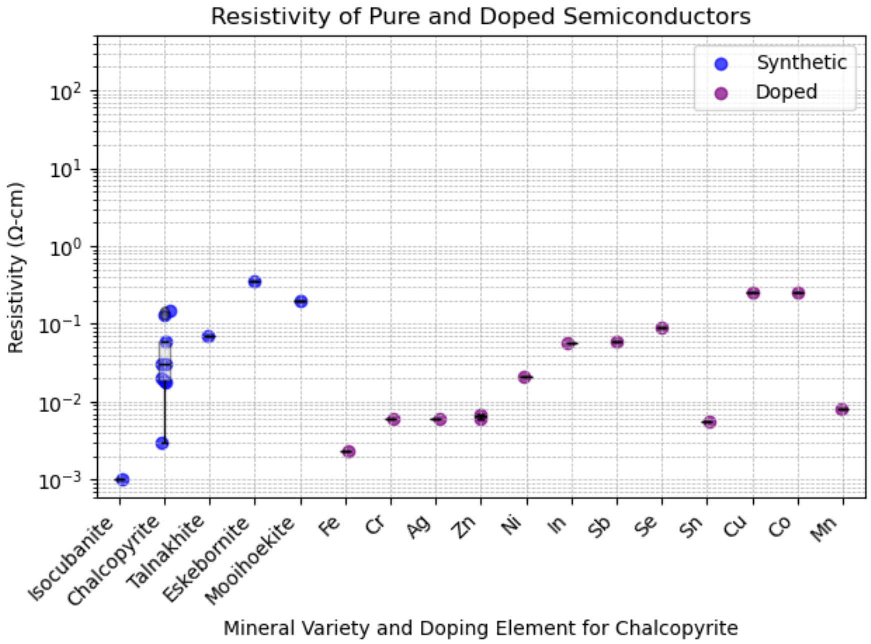

Figure 4 Resistivities of pure synthetic chalcopyrites and close Cu-Fe-S sulfide species (blue), in comparison with the resistivity of chalcopyrite doped with metallic elements at concentrations reported in Table 1 (purple).

Table 1 Synthetic chalcopyrite doped with elements in the concentrations listed. Literature values were selected as the greatest concentration that the chalcopyrite lattice could hold before deformation or exsolution occurred. In the case of incompatible elements like Cr, where all concentrations of an element formed a non-tetragonal structure, the lowest concentration of the element was used.

Element	Dopant	Max Dopant Concentration	Resistivity (Ω-cm)	Reference
Ag-doped cpy	Ag	$Cu_{0.9}Ag_{0.1}FeS_2$	0.006	Ge et al., 2019
Co-doped cpy	Co	$Cu_{0.92}Co_{0.08}FeS_2$	0.25	Berthebaud et al., 2015
Cr-doped cpy	Cr	$CuFeCr_{0.02}S_2$	0.006	Tippireddy et al., 2023
Cu-doped cpy	Cu	$Cu_{1.05}Fe_{0.95}S_2$	0.256	Teranishi & Sato, 1975
Fe-doped cpy	Fe	$Cu_{0.95}Fe_{1.05}S_2$	0.0023	Tsujii & Mori, 2013
In-doped intermediate	In	$CuFe_{0.92}In_{0.08}S_2$	0.059	Xie et al., 2016
Ni-doped cpy	Ni	$Cu_{0.92}Ni_{0.08}FeS_2$	0.021	Kwon & Kim et al., 2025
Sb-doped cpy	Sb	$CuFeS_{1.9}Sb_{0.1}$	0.059	Teranishi & Sato, 1975
Se-doped cpy	Se	$CuFeS_{1.6}Se_{0.4}$	0.09	Carr & Morelli, 2016
Sn-doped cpy	Sn	$Cu_{0.96}Sn_{0.04}FeS_2$	0.0056	Tippireddy et al., 2022
Zn-doped intermediate	Zn	$Cu_{0.97}Zn_{0.03}FeS_2$	0.007	Xie et al., 2017
Zn-doped cpy	Zn	$Cu_{0.97}Zn_{0.03}FeS_2$	0.006	Tsujii & Mori, 2013
Mn-doped cpy	Mn	$Cu_{0.97}Mn_{0.04}FeS_2$	0.008	Lefèvre et al., 2016

Chalcopyrite	None	$CuFeS_2$	0.13	Berthebaud et al., 2015
Chalcopyrite	None	$CuFeS_2$	0.031	Tippireddy et al., 2022
Chalcopyrite	None	$CuFeS_2$	0.031	Tippireddy et al., 2023
Chalcopyrite	None	$CuFeS_2$	0.0204	Ge et al., 2019
Chalcopyrite	None	$CuFeS_2$	0.0188	Xie et al., 2016
Chalcopyrite	None	$CuFeS_2$	0.003	Teranishi & Sato, 1975
Chalcopyrite	None	$CuFeS_2$	0.059	Carr & Morelli, 2016
Chalcopyrite	None	$CuFeS_2$	0.018	Lefèvre et al., 2016
Mooihoekite (CFS-TG)	None	$Cu_9Fe_9S_{16}$	0.2	Shah et al., 2025
Eskebornite	None	$CuFeSe_2$	0.35	Berthebaud et al., 2015
Talnakhite (CFS-HG)	None	$Cu_9Fe_8S_{16}$	0.07	Shah et al., 2024
Isocubanite	None	$CuFe_2S_3$	0.001	Barbier et al., 2017

It is notable that all doped variants remain within the reported range of 0.003 to 0.15 Ω-cm for pure synthetic chalcopyrites, though some are above or below the mode of 0.02 Ω-cm. Six elements increased resistivity (Co, Cu, Sb, Se, In); Se typically substitutes on the sulfur site within chalcopyrite, while In, Co, Cu, and Sb typically substitute for Fe^{3+}. The elements that decreased resistivity (Zn, Ag, Cr, Sn, and Mn) typically substitute for Cu or are interstitial within the chalcopyrite lattice. The element that with the least apparent effect on chalcopyrite resistivity was Ni, which Kwon & Kim (2025) found fit exceptionally well in the chalcopyrite structure.

Overall, current metallurgy research has not characterized trace elements for chalcopyrite; thus, research is unable to connect leaching behavior to any potential influence. The closest comparison is pure and doped chalcopyrite from materials science, although this only provides a frame of reference for whether certain elements raise or lower resistivity and is a poor comparison for any chalcopyrite with numerous substitutions. Experiments on how resistivity impacts leaching is rare and variations have been observed, but dissolution is thought to decrease as resistivity increases due to decreased conductivity (Eghbalnia, 2012; McMillan et al., 1982a; Pridmore & Shuey, 1976). The goal of this project's experiments is to narrow the gap in trace element characterization and bridge the literature between chalcopyrite properties and variability in leaching behavior.

3.0 Methods and Materials

High-grade (>85%) natural chalcopyrite samples from a variety of deposit types were obtained from Ward's Scientific and from existing collections at the University of Arizona. The high-grade samples were not crushed, powdered, or re-pressed in order to avoid affecting exsolution textures, mineralization inclusions, and non-chalcopyrite high-grade sulfides disseminated throughout a typical ore matrix, all of which can affect resistivity (Murr & Hiskey, 1981). These samples, their localities, textures, and additional minerals are described in Table 2.

Table 2 Location, description, identified metal sulfides, and source deposit type of samples analyzed in study. Bn = bornite, py = pyrite, cov = covellite, dig = digenite, sph = sphalerite, apy = arsenopyrite, gal = galena, prg = pyrargyrite, bar = barite, anh = anhydrite, cub = cubanite, ttr = tetrahedrite, ac = acanthite.

Sample	Locale	Texture/description	Deposit Type	Additional Sulfides
JNat1	Ajo Mine, AZ, US	Cpy matrix with py and sph inclusions; minor bn and cov in matrix; trace silicate mineralogy	Porphyry-Cu	bn, py, cov
JNat2				
JNat3				
JNat4				
JNat5		Cpy veining in matrix of qtz and kspar, bn, and py		
JNat12		Cpy matrix; some bn and trace py inclusions; veinlet of digenite w/ bn selvage; some Cu-Ox in Cu-S		bn, py, dig, cov
JNat6	Maria Mine	Cpy matrix with some qtz, trace py, and other trace silicates	Porphyry-Cu	py
JNat17		Cpy matrix with trace acanthite veinlets and trace sph		sph, ac
JNat7	Mission Mine	Cpy matrix with sph exsolutions; trace py; some dol and qtz	Skarn	py, sph
JNat14		Mostly cpy; sample cut by trace cal and qtz veinlets; trace sph		sph
JNat8	Walker Mine, CA, US	Cpy, qtz; trace arsenopyrite and Ag-Sb-S inclusions in qtz veining	Meta-SEDEX	apy, prg
JNat16		Cpy, qtz; trace gal, sph, hem, and Ag-Sb-S inclusions in qtz; some clay/amph silicates		gal, sph, prg
JNat9	Bisbee, AZ, US	Cpy with some py, trace sph and gal inclusions, trace Cu-Sb-S; in Ca-Mn-carbonate w/ trace qtz; trace Cu-As-S	Mississippi Valley Type (MVT) / SEDEX	py, sph, gal, ttr, eng
JNat10	Milpo, Peru	Cpy matrix with noticeable grain boundaries; some amph silicates and barite, trace sph and Fe-Ox	Skarn	sph, bar
JNat11	Ray Mine, AZ, US	Cpy with gal inclusions, sph exsol throughout; cpy veinlet w/ Ag; trace py	Porphyry-Cu	gal, sph, py
JNat15		Cpy matrix; qtz and anhydrite; trace hem, gal, sph, and apatite in sulfide		gal, sph, anh
Nor1	Noranda, Quebec, CAN	Massive cpy with trace sph and py inclusions	Volcanic-hosted	py, sph
Nor2				

JNat13		Massive cpy with trace py and Fe-Ox; trace calciosamarskite	massive sulfide (VMS)	py
Sud1	Sudbury, Ontario, CAN	Massive cpy with trace sph and cub inclusions	Magmatic segregation (MagSeg)	sph, cub
WARDI	Ward's Scientific	Massive cpy cut by minor qtz, (Ca-Fe) pyx, and (Ca-Fe) amph veinlets, and trace sph	Variable, Unknown	py, sph
WARD4-1		Massive cpy with trace sph and py inclusions		
WARD4-2		Massive cpy; trace qtz veinlet breccia with cpy clasts; trace sph and py		

After selection, the chalcopyrite samples were sanded to 2mm level thickness. These were placed in a PCB holder and four probes were placed directly on the sample without silver paste. Hall measurements were taken using an HMS-5000 instrument with 0.55 T magnetic field and 1.00 mA current under ambient pressure and temeprature. Each sample was measured 3 times for 25 rounds apiece at 1 minute intervals. These measurements were averaged to produce a single mobility and resistivity reading. Resistivity (ρ) was calculated as the reciprocal of electrical conductivity (σ) via measurements of the Hall coefficient as shown in Equation 1, where V_H is the Hall voltage, t is the sample thickness, I is the applied current, B is the magnetic field, and ρ is the resistivity.

$$\mu = \frac{\sigma \cdot V_H \cdot t}{I \cdot B} \qquad \sigma: \frac{1}{\rho}$$

Equation 1. Relationship between Hall coefficient and resistivity, and between resistivity and conductivity.

After measurements, each whole-rock chalcopyrite sample was mounted in a 1" round epoxy mount and polished down to 0.25-µm grit. Mounts were photographed in reflected light using a Nikon LV100 petrographic microscope in order to describe textures and verify quantitative results.

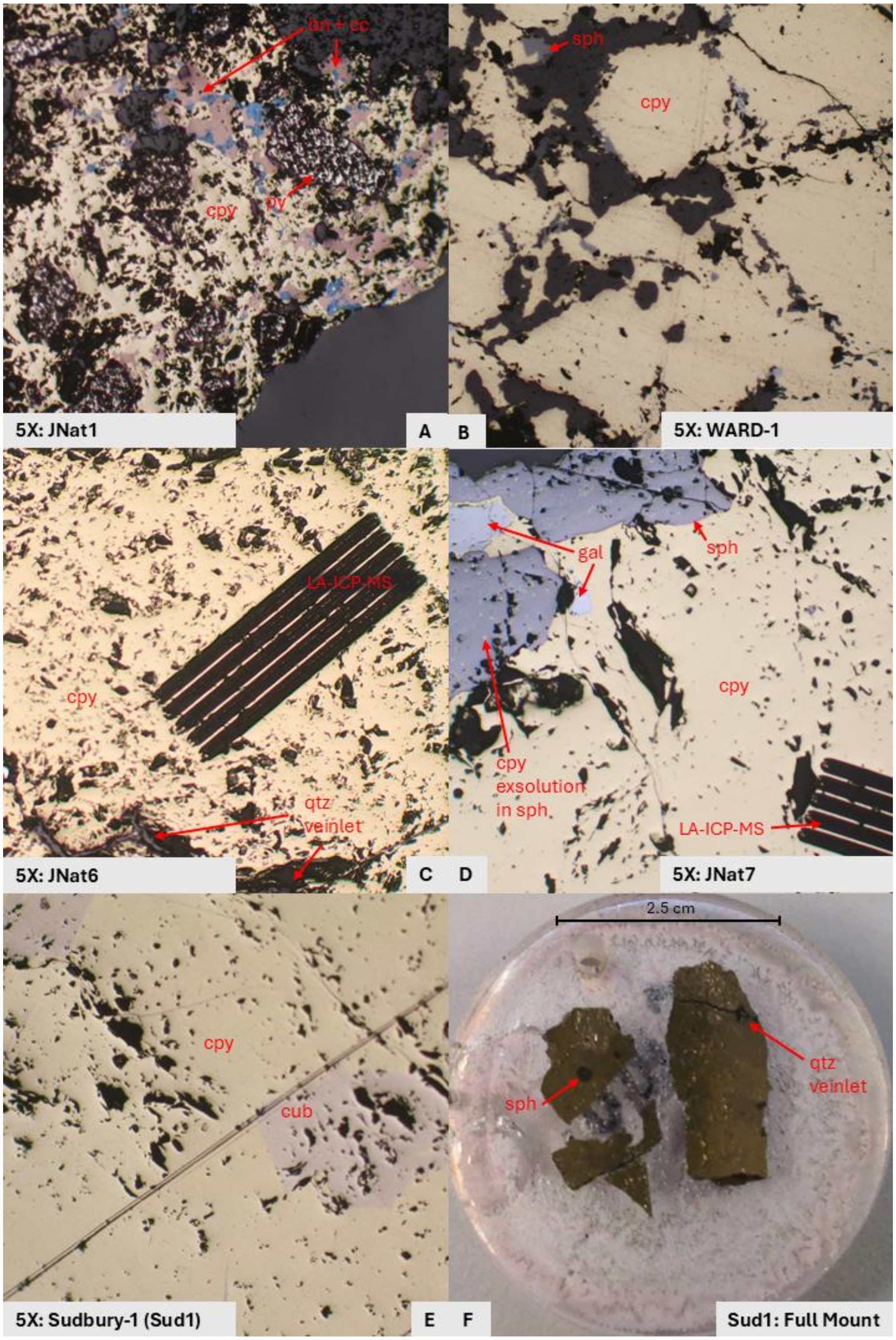

Figure 5 A: Example of numerous bornite (bn), chalcocite (cc), and pyrite (py) inclusions in chalcopyrite (cpy) matrix under reflected light microscopy. B: Chalcopyrite matrix with trace sphalerite (sph) inclusions and trace dark gray quartz (qtz). C: Example of trace quartz (qtz) veinlet near LA-ICP-MS measurements in cpy. D: Example of cpy inclusions in sph and galena (gal) near LA-ICP-MS measurements. E: Example of similarities between cpy and cubanite (cub). F: Full mount of Sud1 where sph is visible, but numerous cubanite inclusions are are nearly invisible, though present.

Sulfides within the mount were analyzed via a Cameca SX100 electron probe microanalyzer (EPMA) and an ESL NWRFemto 257nm Laser Ablation system in the Lowell Minerals Characterization Facility at the University of Arizona. Sulfide mineral identification was conducted visually based on the reflected-light petrography and supported by EPMA analysis. Silicate minerals, if any, were identified through energy-dispersive spectroscopy (EDS) attached to the EPMA. Sulfide concentrations were taken from these analyses, averaged, and normalized based on 4 anticipated ions (1 Cu, 1 Fe, and 2 S) within the crystal structure. However, since most of the trace elements analyzed were below the EPMA detection limits (Appendix B), LA-ICP-MS Femto line measurements were used for all trace element analysis. The microprobe detection limits are reported in Appendix B while the major elements are reported in Table 3, and trace elements in Appendix C. However, in the interest of detecting trends that trace elements might show, only LA-ICP-MS results are reported in Results.

LA-ICP-MS Femto line measurements were calibrated using Iolite 4.0's 3D Trace Element Data Reduction Scheme as developed by Paul et al. (2023). Reference Materials were used by NIST-610 (Norman et al., 1996), MASS-1 (Wilson et al., 2002), STDGL3 (Belousov et al., 2023), and UQAC's CCu-1e, FeS-4, FeS-5, FeS-6, and PTC-1b (Savard et al., 2023), which were correlated to a >0.99 R^2 Ordinary Least Squares fit across each reference material analytical block (four per session) for each element. Laser Raster-line spot size was 65 μm-s^{-1}. with a fluence of 0.84 j-cm^{-2} For NIST-610 and STDGL3, and fluence of 0.14 j-cm^{-2} for all other materials at 1000 hz. Paul et al. (2023) suggested a bracketing procedure which was repurposed with adjustments as two 0.25 mm lines of reference material for every four to five 0.75 mm measurement lines of each sample specimen, and finishing with another run of reference material. Warmup-washout times were 8 ms and 4 ms for each laser line analysis respectively. Helium was the carrier gas for the laser chamber with argon for the ThermoScientific X-SERIES 2 ICP-MS.

Measured isotopes and their dwell times are noted in Appendix A, with a total cycle time of 529 ms. Regions of interest were drawn on calibrated trace element maps with Iolite's Inspection feature, filtering out obvious inclusions of other minerals represented by anomalous element spikes (Drost et al., 2018); the compositions of the regions of interest were then averaged to derive a clean lattice composition of the sample. Trace elements were collected on the Femto only for Cu-Fe sulfides in order to prevent major element contamination from other minerals present in the sample, e.g. galena.

Criteria for genuine correlations between composition and resistivity include a clear positive or negative relationship with $R^2 > 0.5$ and p-value < 0.05. Correlations were considered to exist, but to be modest, with $0.4 < R^2 < 0.5$ and p-value < 0.05. Relationships both with R^2 and p-value near but still below these thresholds ($R^2 > 0.35$, $p < 0.06$) were deemed poor-quality correlations. As an additional check, the R^2 should be similar for multiple elements with similar valence and crystallographic site.

4.0 Results

The average major-element compositions, resistivities, and charge mobilities measured from samples in this study are shown in Table 3. Table 4 contains average trace-element compositions. Full data is in Appendix C.

Table 3 Average normalized EPMA weight percent major elements for chalcopyrite from each sample, along with average resistivity and charge mobility measurements. For raw data and analytical totals, see Appendix. Italicized values denote results that are suspect due to anomalies during measurement.

Sample	Deposit Type	Cu (mol)	Fe (mol)	S (mol)	Cu (wt%)	Fe (wt%)	S (wt%)	Avg Resistivity, Ω-cm	Avg Mobility, $cm^2V^{-1}s^{-1}$
JNat1	Porphyry	1.00	1.00	2.00	34.46	30.51	34.89	0.17	26.10
JNat2	Porphyry	1.02	1.02	1.96	34.56	30.22	33.51	2.35	2.93
JNat3	Porphyry	1.01	1.01	1.98	34.48	30.44	34.19	0.16	22.73
JNat4	Porphyry	1.00	1.01	1.99	34.53	30.43	34.53	0.17	28.92
JNat5	Porphyry	1.00	1.01	1.98	34.41	30.45	34.28	6.87	4.87
JNat6	Porphyry	1.00	1.01	1.99	34.58	30.53	34.62	*8.11E+04*	0.33
JNat7	Skarn	1.01	1.01	1.98	34.65	30.52	34.49	4.63	10.89
JNat8	Meta-SEDEX	1.00	1.01	1.99	34.24	30.45	34.54	0.14	141.01
JNat9	SEDEX	1.00	1.00	2.00	34.53	30.38	34.87	*5.75E+06*	0.11
JNat10	Skarn	1.00	1.01	1.99	34.68	30.63	34.83	0.27	14.27
JNat11	Porphyry	1.00	1.01	1.99	34.59	30.48	34.54	0.83	11.77
JNat12	Porphyry	1.01	1.00	1.99	34.67	30.31	34.54	0.70	4.25
JNat13	VMS	1.00	1.01	2.00	34.63	30.72	35.02	0.02	128.86
JNat14	Skarn	1.00	1.00	2.00	34.56	30.48	34.81	4.57	15.26
JNat15	Porphyry	1.00	1.00	1.99	34.69	30.55	34.78	1.68	13.92
JNat16	Meta-SEDEX	0.99	1.02	1.98	34.26	30.89	34.53	0.05	30.83
JNat17	Porphyry	1.00	1.01	1.99	34.59	30.54	34.67	0.09	24.47
Nor1	VMS	1.00	1.02	1.97	34.31	30.56	34.04	0.02	48.99
Nor2	VMS	1.00	1.03	1.97	34.22	30.83	34.02	0.35	6.08
Sud1	MagSeg	1.00	1.01	1.99	34.41	30.73	34.63	1.77	0.96
WARDI	Unknown	1.00	1.01	1.99	34.37	30.51	34.66	30.62	0.75
WARD4-1	Unknown	1.00	1.01	1.99	34.68	30.58	34.73	0.94	9.17
WARD4-2	Unknown	1.00	1.00	1.99	34.79	30.63	34.86	1.50	4.35

As the box-and-whisker plot in Figure 6 shows, obtained data falls largely within the range of resistivities exhibited by natural chalcopyrite samples reported in the literature. While variation is considerable, chalcopyrite from the same deposit types show similar tendencies as reported in the literature. The upper outlier for magmatic segregation (MagSeg) is from Sudbury, used by Telkes (1950), and is nearly the same value as this study's Sudbury sample. Walker Mine, which was classified as a metamorphic sedimentary (meta-SEDEX) deposit type, shows values similar to both Meta-SEDEX and SEDEX. Noranda, which is classified as a volcanic massive sulfide (VMS) deposit, is also similar to reported values for other VMS's. Notably, samples JNat6 and 9 from Table 3 have extremely high resistivities which fall outside the range of previously measured values for natural and synthetic chalcopyrites (Figure 6). While JNat9 does show unusual trace element values, both samples also show large standard deviations compared to other measurements in this study. Thus, these measurements are attributed to poor Hall measurement and have been excluded from further graphs and discussion.

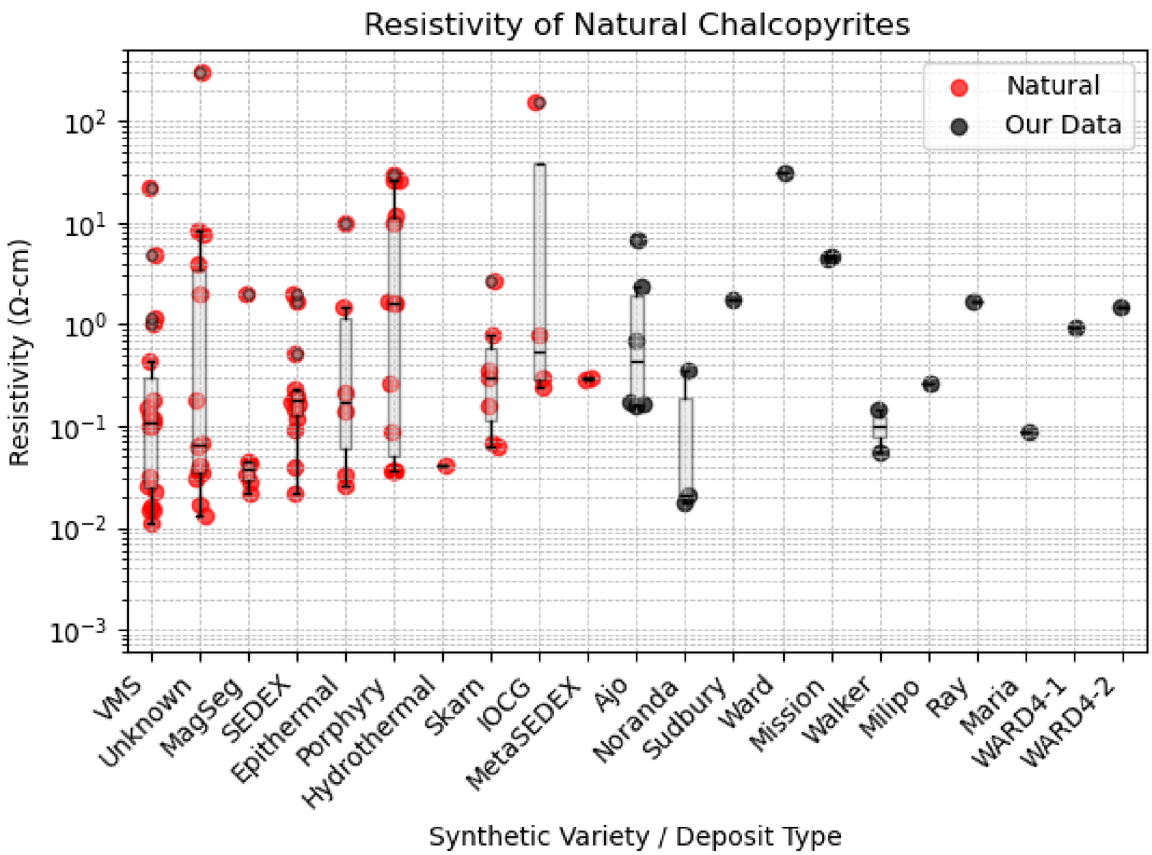

Figure 6 Resistivities of natural chalcopyrites compiled from literature (red) and resistivities of chalcopyrite used in this study (gray). Figure after data compiled by (Barton & Hiskey, 2022b).

For easier visualization of the major-element compositions of the samples in this study, the Fe, Cu, and S weight percentages were plotted on a graphical ternary diagram in Python against reference points of published Cu-Fe-S mineral compositions (Ralph et al., 2025). The results (Figure 7) show that the samples in this study almost all fall cleanly in the chalcopyrite range, with the exception of some cubanite in Sud1, a mooihoekite-putoranite in Nor1, and an unknown phase of intermediate composition in WARD1. However, only JNat1, JNat9, and JNat14 are exact stoichiometric matches for chalcopyrite (Table 3). The remainder are nearly all undersaturated in S relative to metals, and most also have a slight excess of Fe relative to Cu.

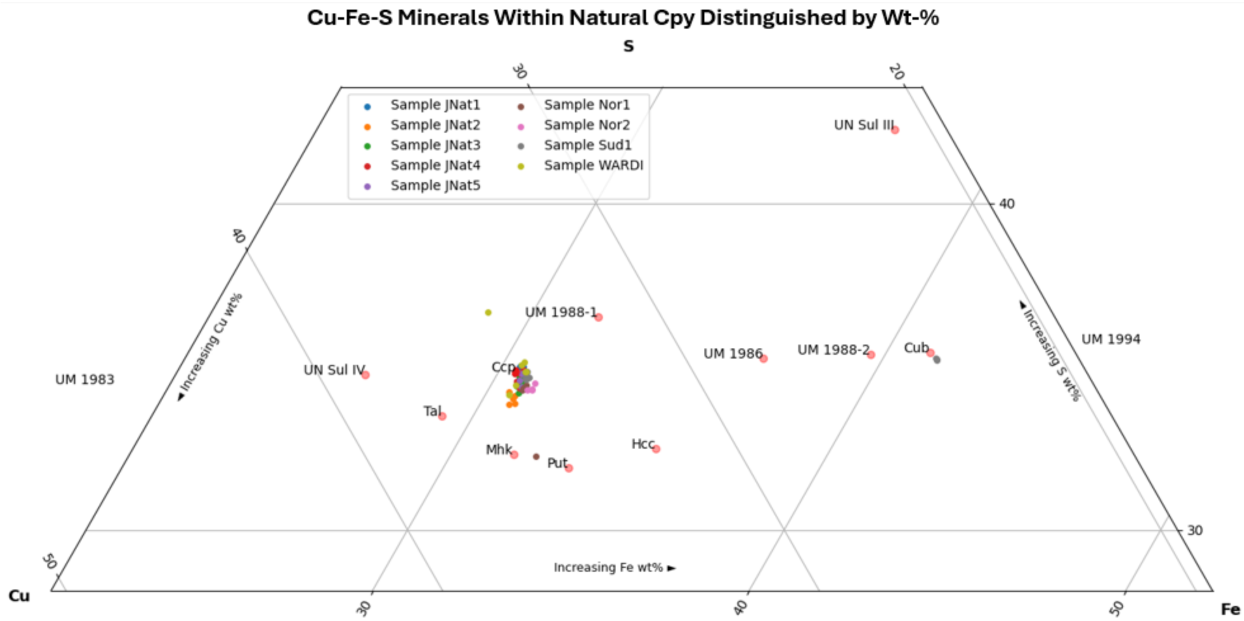

Figure 7 Ternary diagram plotting reference minerals in the Cu-Fe-S system along with wt-% measurements of Cu-Fe-S minerals in this study. Chalcopyrite (cpy alt: ccp), talnakhite (tal), mooihoekite (mhk), puteranite (put), haycockite (hcc), cubanite (cub). UM and UN are unnamed, rare Cu-Fe-S mineral variations that have only been found once in nature, denoted by their publishing year or Mindat "Sul IV" notation (Mindat.org, 2025) following the nomenclature of the International Mineralogical Association. Additional information on the compositions of minerals in the Cu-Fe-S system is available from Barbier et al. (2017); Barton (1970); Fleet (1970).

Major-element compositions were measured by EPMA and shown in Table 3. The corresponding analyses measured by femtosecond LA-ICP-MS are in Table 4. No correlation was observed between major-element ratios (Cu/S, Fe/S, or (Cu+Fe)/S) and resistivity (Figure 8).

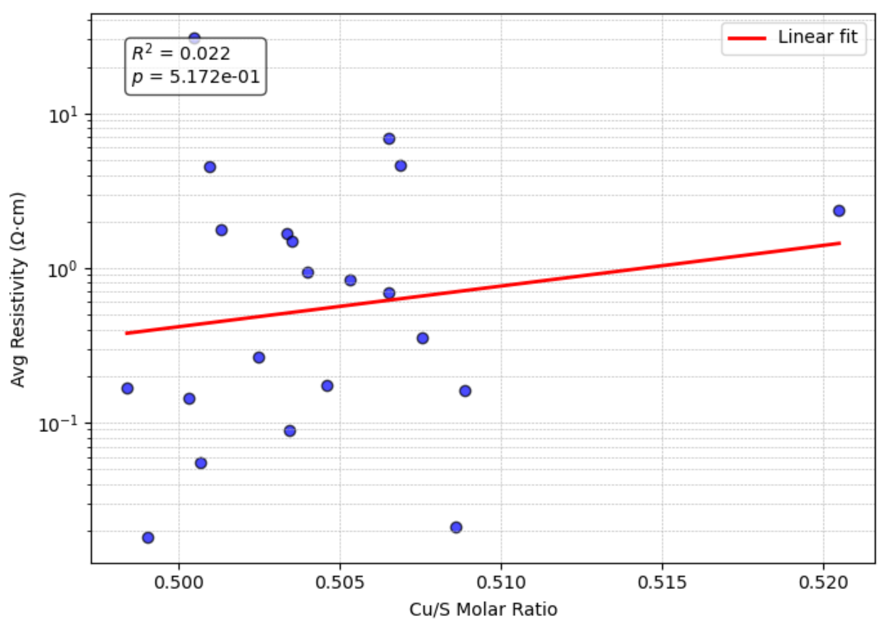

Figure 8 Ratio of normalized major elements obtained by the EPMA in Table 3, to resistivity (Ω-cm).

Table 4 Averaged trace element concentrations in chalcopyrite in this study from LA-ICP-MS analysis. Dashes replace analyses eliminated as unreliable.

Sample	Zn	Ga	Ge	As	Se	Ni	Co	Ag	In	Te	V	Sn	Hg	Bi	Pb	Sb	Mn	Cd	Au	Cr	Mg
Units	*ppm*	*ppm*	*ppm*	*ppm*	*ppm*	*ppm*	*ppm*	*ppm*	*ppm*	*ppm*	*ppm*	*ppm*	*ppm*	*ppm*	*ppm*	*ppm*	*ppm*	*ppm*	*ppm*	*ppm*	*ppm*
JNat6	0.0	7.4	0.9	0.5	94.7	829.4	0.0	32.5	32.7	0.0	5.5	84.9	1.2	57.1	1.8	2.2	45.9	10.3	8.3	45.1	1.7
JNat7	0.0	6.7	0.6	1.4	64.5	1369.1	152.1	102.3	10.1	0.0	4.9	21.9	0.1	63.9	31.0	0.4	45.6	6.4	9.0	45.9	5.1
JNat8	136.8	6.3	0.6	0.1	85.4	1108.5	0.0	205.9	2.0	0.0	5.3	11.0	2.7	56.9	3.2	2.5	44.7	28.5	8.7	45.3	6.7
JNat9	0.0	7.5	0.8	2.1	14.2	603.6	0.0	21.0	79.3	3.1	14.5	134.9	0.5	61.6	552.6	6.1	40.0	7.3	4.0	58.0	1.2
JNat10	321.8	4.3	2.1	71.4	209.4	1960.5	0.0	16.2	7.3	0.0	3.5	71.7	0.1	31.1	1.8	0.0	112.1	19.3	5.9	0.0	0.8
JNat11	0.0	2.1	2.8	73.7	346.3	1904.1	0.0	18.5	0.2	0.0	3.1	18.0	0.0	31.5	18.0	0.1	118.6	0.1	6.0	0.0	0.2
JNat12	0.0	0.8	0.0	76.7	44.1	1725.6	0.0	17.9	0.4	0.0	16.2	18.4	0.1	28.1	348.8	2.8	129.4	0.0	6.2	0.0	52.5
JNat13	0.0	35.1	4.3	74.4	601.1	1833.2	0.0	164.9	74.5	0.0	2.7	49.7	0.1	43.3	1.9	0.6	116.9	0.3	6.5	11.1	1.7
JNat14	0.0	2.5	2.3	72.2	35.6	1903.9	150.3	96.6	12.8	0.0	3.0	25.3	0.0	39.3	36.2	0.5	115.0	0.0	6.6	0.0	21.4
JNat15	507.3	4.2	1.3	66.2	247.9	1965.0	0.0	20.0	8.5	0.0	3.2	80.2	0.9	34.4	1.6	0.0	111.7	23.4	6.7	0.0	0.1
JNat16	0.0	2.2	3.8	75.9	87.8	1841.7	0.0	243.6	2.4	0.0	3.1	16.6	2.7	32.7	5.4	2.9	117.4	25.0	6.2	10.3	0.1
WARD4-1	0.0	6.0	12.9	29.6	112.9	-	5.1	10.3	11.8	0.0	6.7	0.9	0.0	0.9	32.9	5.2	21.4	12.1	4.6	0.3	0.0
WARD4-2	0.0	5.0	10.1	23.6	27.8	-	127.0	54.9	17.2	0.0	6.3	7.7	0.0	3.0	52.1	5.1	18.3	1.5	4.0	0.1	0.0

Table 4 shows some notable features, particularly the high concentrations of Ni observed in all samples. These are almost certainly due to analytical artifacts and not to high Ni in the samples. Figure 9 shows an example of the elemental mapping carried out by LA-ICP-MS in the study, illustrating the clearly anomalous behavior of Ni. Lesser analytical peculiarities were noted in the maps generated for Au and Cr, although the Au map does show some real features such as the Ag-As-rich vein in the lower right.

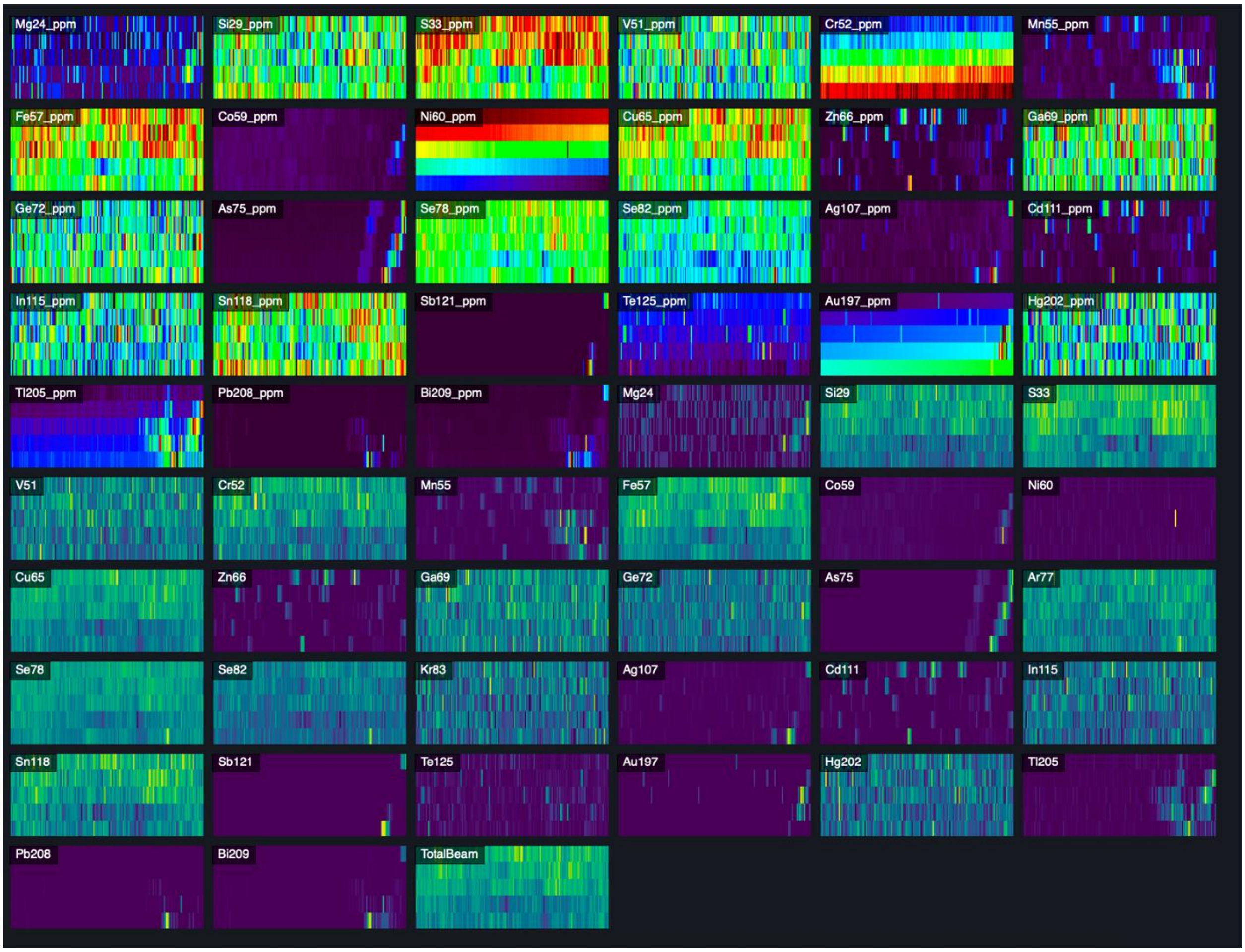

Figure 9 Map of elemental distribution in an area of sample JNat11, generated by LA-ICP-MS. Higher concentrations are shown in warmer colors, scaled to each element's abundance. Isotopes subscripted _ppm are unprocessed; isotopes without subscripts show the distribution of the element after processing the data.

For each averaged sample, ppm values from LA-ICP-MS (Table 4) were plotted against the resistivity calculated from Hall measurements (Equation 1). Each graph was examined for correlation using R^2 and p-value as described in Methods and Materials.

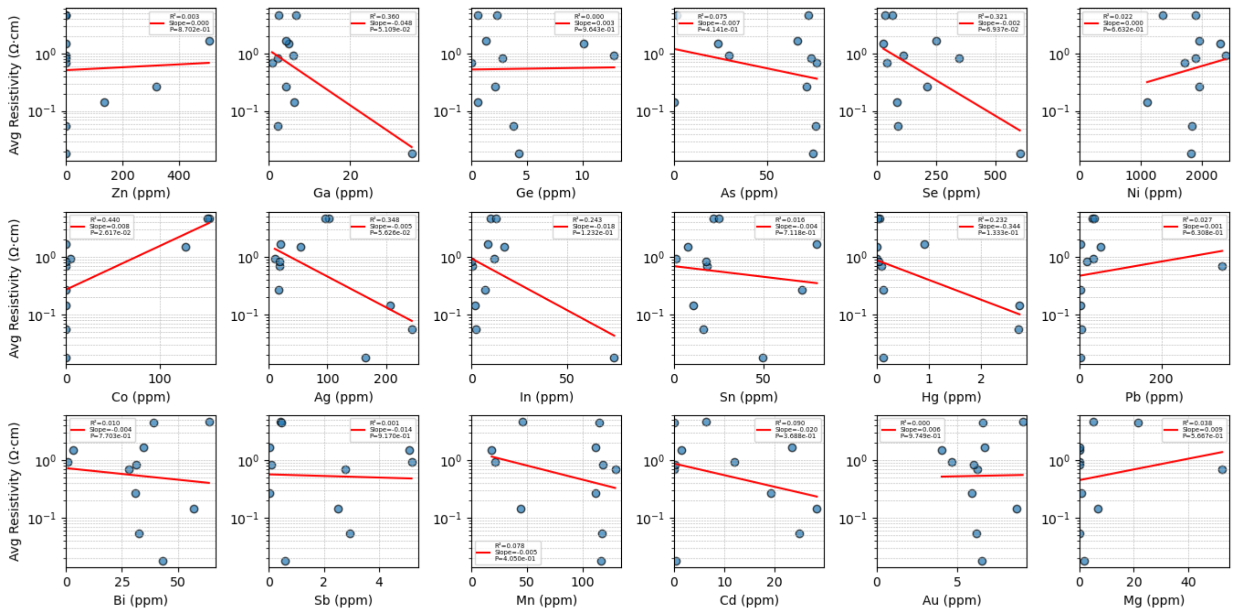

Figure 10 Trace element data obtained from LA-ICP-MS in ppm set against log-scale resistivity (Ω-cm) on all y-axes. Te was removed from the graphs as it was only detected in the potentially erroneous JNat9.

The relationships of LA-ICP-MS measurements of individual trace elements to resistivity are variable and mostly below the criteria for correlation. The highest R^2 value is 0.440 for Co, followed by Ga, Ag, Se, In, and Hg at $0.3 < R^2 < 0.4$. All other correlations show an R^2 of < 0.1. No correlation other than Co was deemed statistically significant based on p-value.

Correlations were also sought based on two different combinations of elements. In grouping scheme #1, trace elements were compartmentalized by the known or estimated ion substitution position within the chalcopyrite's lattice in nature (Table 6). Nickel and cobalt were assigned to the Fe site despite synthetic experiments substituting them for Cu (Kwon & Kim, 2025), since they have more charge and radius similarity to Fe^{3+} than to Cu^{+} and naturally substitute for Fe in talnakhite and pyrite respectively. Indium was placed in the Fe site as indicated by experiments on synthetic chalcopyrite and the existence of the mineral roquesite ($CuInS_2$). Germanium and gallium were also placed in the Fe site due to the natural minerals calvertite ($Cu_5Ge_{0.5}S_4$) and gallite ($CuGaS_2$). Bismuth was placed in the Fe site as it is generally trivalent, and Cu-Bi sulfides are known. Both Mn and Cd were classified as interstitial based on observations by Yevstigneyeva et al. (1973). Several elements analyzed could feasibly fit in multiple crystallographic sites. Lead can fit in interstices and in the Fe site depending on coupled substitutions with other elements. Arsenic was assigned to both the Fe and S sites as it forms a wide variety of Cu-Fe-As-S minerals and can act as a cation or anion depending on its valence state and the availability of sulfur. Antimony could technically fit in the Cu, Fe, or S sites, but was placed in the Fe site as most natural Sb is trivalent (despite Sb being substituted for S in synthetic chalcopyrite).

In grouping scheme #2, siting was ignored (except for interstitial elements) and ions were grouped based on charge alone (Table 5).

Table 5 Grouping schemes used in seeking multi-element correlations with resistivity.

Grouping Scheme 1	Ion	Elements	Name in graphs
	Cu^{+}	Zn, Ag, Sn, Hg, Cd	Cu_Site
	Fe^{3+}	Ni, In, Ge, Ga, As, Co, Pb, Bi, Sb	Fe_Site
	S^{-2}	Se, Te, As	S_Site
	Interst.	Cr, Au, Mn, Mg, Pb	Interst
	AllCat	All elements in Cu and Fe sites	AllCat
Grouping Scheme 2	**Charge**	**Elements**	**Name in graphs**
	+1	Ag, Hg	CC1
	+2	Ni, Co, Zn, Mn, Cd, Pb, Mg	CC2
	+3	Ga, In, Tl, Bi, Sb	CC3
	+4	Sn, Ge	CC4
	Interst.	Au, Cr	CC5
	-2	Se, Te	AN1
	-3	As	AN2
	AllCat	All +1, +2, +3, and +4 ions	AllCat
	AllAn	All -2 and -3 ions	AllAn

The results for Grouping Scheme #1 are shown in Figure 11. The LA-ICP-MS results show some correlations with resistivity for substitutions in the S site, with $R^2 = 0.321$ and $p = 0.069$. While better trends may emerge with more data, the current results are poor, and the results for S_Site are still not statistically significant.

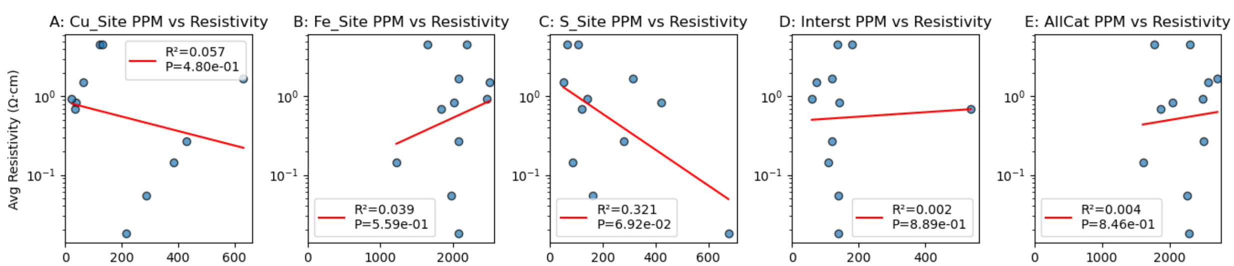

Figure 11 Sum of LA-ICP-MS elements grouped by site (ppm) vs sample resistivity (Ω·cm). Classifications are shown in Table 5, Grouping Scheme #1.

In grouping scheme #2, it is again the anions that show the most consistent (or least inconsistent) relationships with resistivity (Figure 12). The all-anions category shows an $R^2 = 0.321$, $p = 0.069$; the anions with -2 charge contribute significantly with a greater ppm count. However, cations with a +3 charge and +1 charge also show some correlation with $R^2 = 0.242$ and $R^2 = 0.348$ respectively. Neither was statistically significant by p-value, though +1 cations came close with $p = 0.056$ (Figure 12). Thus, neither cation nor anion groups are statistically significant, and all other groups have an R^2 of < 0.1.

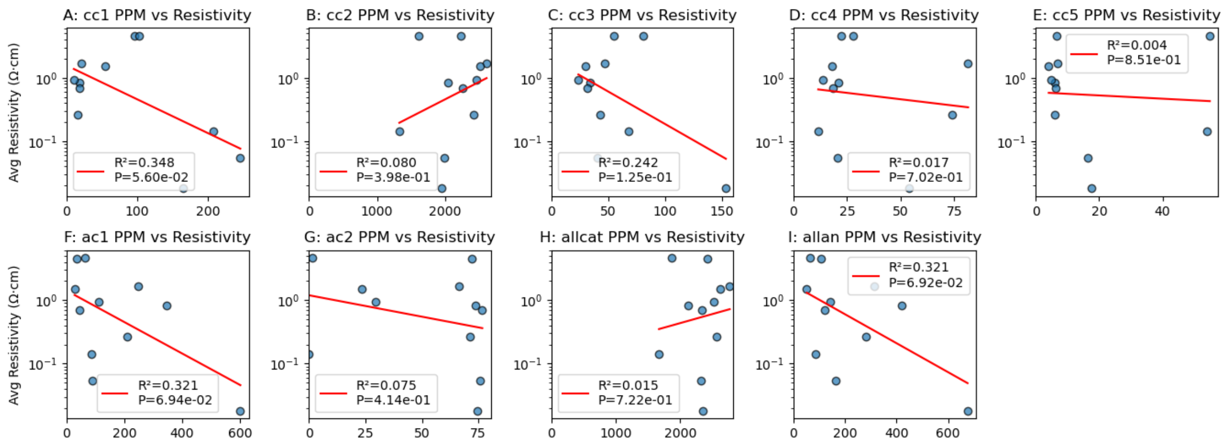

Figure 12 Sum of LA-ICP-MS elements grouped by charge (ppm) vs sample resistivity (Ω·cm). Classifications are shown in Table 5, Grouping Scheme #2.

5.0 Discussion

5.1 Correlation of resistivity with composition

Overall, some trends are visible in this study and indicate a likely connection between chalcopyrite's composition and resistivity. The only element that correlates with resistivity on an individual basis is Co, which is higher in more-resistive samples. This is similar to the findings of Lefevre et al. (2016), whose synthetic chalcopyrites had high resistivities when doped with Co. Otherwise, substitution into a specific site tends to show greater influence on resistivity than the concentrations of individual elements. In particular, substitutions into the S-site had the greatest influence (or perhaps least conflicting influence) on resistivity from the data. This is corroborated by the observations in synthetic samples, particularly by Lefèvre et al. (2016), who notes that greater sulfur deficiency – presumably corresponding to other elements occupying the S site – decreases resistivity, even in doped samples. In practice, the lack of Te in the samples means that the principal effects on resistivity are coming from Se and As (Table 5). However, comparisons with the literature give conflicting results. Increasing Se increased resistivity for doped synthetic chalcopyrite, while increasing Se in natural samples decreased resistivity. This may be due to the potential for coupled substitutions in natural chalcopyrite compared to synthetic variants. Increased concentrations of an alternate cation in Se-rich natural samples could have a countervailing relationship to resistivity. Another possibility is that the effects of Se vary with the presence or concentration of As, or an increase of interstitial elements due to these lattice substitutions.

Otherwise, the least-conflicting correlation was with 1+ cations (Figure 12). The main contributor to this is Ag^{+}. These preliminary results support a potential link between Ag concentration and resistivity, perhaps related to the hypothesized catalytic effect of Ag on chalcopyrite leaching (e.g. Hiroyoshi et al., 2002). However, more work with a larger number of samples would be required to confirm or refute this, along with the possible correlation of resistivity with Co concentration.

In any case, both this study and prior research indicate that connections do exist between trace elements and semiconducting properties. However, they are not obvious or simple. The poor to moderate correlations for all elements analyzed show that there are likely more variables involved, and a more complex relationship, than previously assumed. A likely possibility is that the net semiconducting behavior of natural chalcopyrite is a function of multiple compositional factors acting in concert, along with confounding effects from crystal structure and associated sulfides.

5.2 Sources of complication and inconsistency

One source of inconsistencies in the data was likely from differences of scale among the various characterization techniques applied. The smallest area the 4-probe can measure is 3 mm^2. Finding an area of pure, inclusion-free, homogeneous chalcopyrite this size in a natural sample is nearly impossible. Even the LA-ICP-MS maps in Figure 9 show one veinlet when covering only a fraction of the 4-probe area. Thus the areas analyzed by EPMA, LA-ICP-MS, and the 4-probe station are substantially different. This may influence results and be the cause of large discrepancies in readings, such as JNat 6 and 9.

Additionally, points taken by the EPMA were scattered throughout the chalcopyrite matrix in order to identify potential similar Cu-Fe sulfides and construct an average major-element analysis. Due to the small size of an EPMA spot, these analyses typically represent pure chalcopyrite. While points were often taken near the LA-ICP-MS analysis, it was not possible to analyze the same spot with both methods due to ablation damage and the disturbance to the flat surface. Using the line method on the LA-ICP-MS produced a representative analysis of chalcopyrite, albeit with small and removable inclusions. However, its cumulative area is 0.24 mm^2, which is 3% of the 4-probe's scale. Figure 13 illustrates the difference in size between all these methods and regions of probable inconsistency.

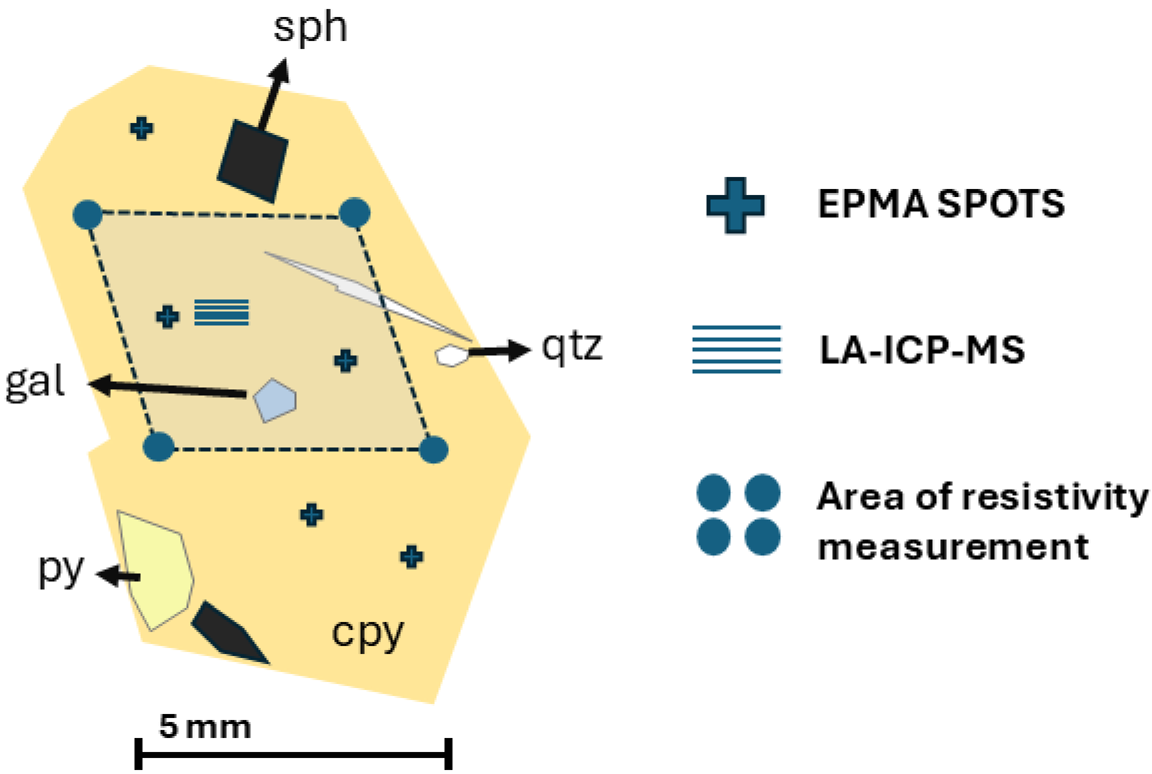

Figure 13 Example of typical chalcopyrite (cpy) sample with EPMA, LA-ICP-MS, and Hall measurements while avoiding (or unable to avoid) interference from common inclusions galena (gal), quartz (qtz), sphalerite (sph), pyrite (py).

The small number of samples is also partly responsible for the lack of strong correlations. Large variations between trace element concentrations are known to occur between deposit types due to trace element partition between mineral species, and the samples selected for this study consist of multiple deposit types. It is likely that better correlations would emerge with either a larger dataset, or a dataset of the same size that only included samples from a single deposit type.

5.3 Implications for leaching

For chalcopyrite leaching, these results could suggest that attempts to consider the impact of trace elements on an individual basis may be fruitless. More likely, the observed variability in chalcopyrite's leaching behavior arises from a complex combination of multiple elements. The most important factor identified is substitution in the sulfide site, but this is only a preliminary analysis. Similarly, attempts to harness single elements (e.g. Ag) to understand good or bad leaching recovery may meet with little success. If resistivity is in fact a function of several different elements and other factors, as this preliminary analysis indicates, then leaching rates may well be too.

Of particular note is the apparent role of elements substituting on the S site. One hypothesis advanced for passivation is the development of an S-rich, p-type surface layer that creates a depletion region. The higher rates of substitution on the S site, which presumably mean lower S relative to metal, may simply inhibit the development of an S-rich layer to some extent, mitigating the effects of passivation. However, this is highly speculative and requires further investigation.

What is clear is that chalcopyrite from different mines and ore deposits has strongly varying characteristics and will probably yield highly variable results when leached with the same lixiviants. It is possible that the chalcopyrite from a particular deposit type shows promising composition and resistivity and will be amenable to leaching, while different chalcopyrite may not. Tentatively, if the resistivity of a chalcopyrite is low due to a high level of relevant trace element substitutions, it could be enough to prevent passive behavior or passivation, allowing the chalcopyrite to fully leach. Further research with a larger suite of samples is necessary to investigate these theories, coupled with electrochemical leach testing.

6.0 Conclusions

Chalcopyrite is an important ore mineral for copper production despite its expensive and intensive sulfide mineral processing requirements. Some research has been done into the nature of synthetic chalcopyrite as a semiconductor. This project builds on that foundation with new analyses to understand how the trace element characteristics of natural chalcopyrite affect its resistivity, and what that implies for leaching behavior.

While it's clear that trace elements are connected to the semiconducting properties of chalcopyrite and are able to influence their resistivity and probably thus dissolution, the only correlation found between resistivity and individual trace elements was a positive relationship between Co and resistivity. Small correlations were noted when trace elements were grouped based on which site they substituted into. The concentrations of elements that substitute onto the S-site appeared to have a particularly noticeable effect. Higher concentrations of these elements typically correlate with a decrease in resistivity. This decrease is similar to the decrease observed in the resistivity of S-poor synthetic samples and could correspond with the development of an S-rich, p-type diode on the surface, possibly implicated in passivation.

Future research includes increasing the number of samples and conducting the same study, comparing inter-deposit type variation by collecting chalcopyrite samples from one or two types of deposit (ex. porphyry or VMS), conducting electrochemical leach tests on the characterized samples, and investigating the impact of cation substitution in relation to anion substitution.

7.0 Appendix A

Table 6 Major and trace isotopes measured via LA-ICP-MS and respective dwell times.

Element	Mg24	Si29	S33	V51	Cr52	Mn55	Fe57	Co59	Tl205
Dwell Time (ms)	*10*	*2*	*25*	*10*	*20*	*10*	*25*	*20*	*10*
Element	**Ni60**	**Cu65**	**Zn66**	**Ga69**	**Ge72**	**As75**	**Au197**	**Hg202**	**Pb208**
Dwell Time (ms)	*20*	*25*	*25*	*10*	*10*	*25*	*10*	*25*	*10*
Element	**Se78**	**Se82**	**Ag107**	**Cd111**	**In115**	**Sn118**	**Sb121**	**Te125**	**Bi209**
Dwell Time (ms)	*25*	*25*	*25*	*10*	*10*	*25*	*10*	*25*	*20*

8.0 Appendix B

Table 7 Table of averaged EPMA detection limits for each sample.

Sample	Zn	Ga	Ge	As	Se	Ni	Co	Ag	In	Te	Sn	Hg	Bi	Pb	Sb	Mn	Cd	Au	Cr	Mg
Units	*ppm*	*ppm*	*ppm*	*ppm*	*ppm*	*ppm*	*ppm*	*ppm*	*ppm*	*ppm*	*ppm*	*ppm*	*ppm*	*ppm*	*ppm*	*ppm*	*ppm*	*ppm*	*ppm*	*ppm*
JNat1	550	740	660	514	994	311	287			360	273	916	833		284	277	602	731		
JNat10	572			380	343	318		323	440	355	279	889			282	289	506	687	215	191
JNat11	572				339	321		319	438	358		917	884		280	282	489	704	219	202
JNat12	562			377	338	318	297	316	444	358	280	903			283	284	506	720	219	194
JNat13	574			378	338	319	299	323	443	356	278	911	888		282	281	508		219	200
JNat14	570			381	343	320	297	319	438	359	278	871	869		280	286	515	716	217	200
JNat15	569			381	343	317	298	323	432	359	279	908	905		280	285	500	709	217	197
JNat16	565			380	342	321	301	322	440		278	919	898			286	506	712	209	197
JNat17	573			577	369	319	295	316	440	358	279	900	893		281	283	498		220	194
JNat2	552	779	662	529	995	308		321		357	278	909			281	276	587	729		
JNat3	554	765	680	522	1022	307	289	319		356	278	912	861		281	274		719		
JNat4	550	760	649	500	1002	309	285	317		353	275	917	874		280	274	577	692		
JNat5	550	758		522	972	307		317		359	276	922	857		277	279	573	735		
JNat6	570			382	341	318	298	319	435	360	279	923	903		284	283	497	670	219	200
JNat7	567			378	338	318	296	318	435	360	274	898	895		281	284	489	701	219	203
JNat8	569			390	344	316	294	316	438	355	278	927	881		281	283	499	701	219	200
JNat9	569			380	338	318	297	314	435	358	276	915	900	1163	281	283	503	729	220	197
Nor1	551	771	679	509	1011			325		358	277	923	865		279	279	588	736		
Nor2	553	771	646	526	1006	307	287	316		357	280	910	861		283	280	582			
Sud1	550	755		518	1013	308	292	315		360	276	923			283	277	600	695		
WARD4-1	780			724	664	444	413	432		501	393	1261	1238		394	384	822	970	303	274
WARD4-2	773			722	655	443	411	434		502	387	1271	1185		385	380	830	973	291	272
WARDI	556	791	677	526	1023	311	288	324		360	279	921	859		284	281		736		
AVG	**580**	**765**	**665**	**477**	**629**	**326**	**307**	**329**	**438**	**371**	**288**	**942**	**913**	**1163**	**291**	**290**	**561**	**738**	**229**	**209**

9.0 Appendix C

Table 8 Average EPMA ppm values from given chalcopyrite samples. The only Pb value recorded by the EPMA was in JNat9, which returned a large standard deviation of error and has been excluded from further graphs and discussion. Major elements for samples are reported in Table 3.

Sample	Zn	Ga	Ge	As	Se	Ni	Co	Ag	In	Te	Sn	Hg	Bi	Pb	Sb	Mn	Cd	Au	Cr	Mg
Units	*ppm*	*ppm*	*ppm*	*ppm*	*ppm*	*ppm*	*ppm*	*ppm*	*ppm*	*ppm*	*ppm*	*ppm*	*ppm*	*ppm*	*ppm*	*ppm*	*ppm*	*ppm*	*ppm*	*ppm*
JNat1	9.48	3.11	0.88	1.77	3.87	0.31	0.41	0.00	0.00	0.26	1.47	2.96	0.45	0	0.19	2.62	0.22	0.64	-	-
JNat10	10.20	-	-	1.05	2.84	0.61	0.00	0.49	2.06	1.60	0.62	3.37	0.00	0	0.43	0.94	1.02	0.95	0.99	6.45
JNat11	11.04	-	-	0.00	5.37	0.21	0.00	1.67	1.14	0.43	0.00	1.14	0.34	0	0.11	2.79	2.50	0.94	1.53	4.70
JNat12	8.28	-	-	1.27	2.32	2.31	0.73	0.68	1.41	0.38	0.16	1.76	0.00	0	0.03	1.98	1.91	0.03	1.26	5.03
JNat13	11.31	-	-	3.48	7.80	0.42	0.37	2.38	1.79	0.57	0.59	2.86	0.18	0	0.27	3.86	2.05	0.00	0.86	2.70
JNat14	6.59	-	-	1.18	0.42	0.65	0.75	0.90	2.09	0.33	0.49	3.94	0.31	0	0.25	1.97	0.82	0.40	0.69	3.18
JNat15	31.72	-	-	2.20	3.48	2.68	0.67	1.20	2.16	0.30	1.57	3.23	0.43	0	0.74	2.46	2.58	0.53	1.24	2.95
JNat16	20.76	-	-	1.93	2.92	1.44	0.19	3.28	0.77	0.00	0.49	1.96	0.43	0	0.00	2.23	1.86	0.75	1.13	2.98
JNat17	8.78	-	-	13.38	2.35	1.03	0.84	1.47	1.93	0.72	1.08	3.87	0.11	0	0.24	2.12	3.26	0.00	0.76	6.34
JNat2	7.27	1.14	1.22	1.77	2.44	1.34	0.00	1.07	0.00	0.33	0.38	2.56	0.00	0	0.50	2.79	0.43	0.31	-	-
JNat3	7.89	5.52	0.24	0.74	2.10	1.68	1.67	0.88	0.00	0.70	0.27	1.62	0.11	0	0.22	1.53	0.00	1.06	-	-
JNat4	8.68	2.78	0.55	1.70	2.54	1.00	0.58	0.44	0.00	0.51	0.56	1.67	0.23	0	0.48	2.85	2.08	1.17	-	-
JNat5	9.65	2.30	0.00	2.32	4.26	1.00	0.00	0.99	0.00	0.49	1.00	1.52	0.18	0	0.69	0.47	1.73	1.64	-	-
JNat6	15.18	-	-	1.01	0.58	0.79	0.20	1.28	2.73	0.22	0.56	2.08	0.17	0	0.40	2.01	3.46	0.64	0.49	3.02
JNat7	7.25	-	-	0.43	1.87	1.43	0.43	1.56	2.33	0.03	0.25	3.52	0.54	0	0.21	2.09	2.74	0.75	1.23	0.70
JNat8	14.17	-	-	0.20	1.20	1.37	0.75	14.38	1.68	0.60	0.68	0.66	0.73	0	0.15	3.01	2.93	0.65	0.28	2.69
JNat9	9.32	-	-	1.81	1.44	1.44	0.39	2.87	2.33	0.69	2.11	2.01	0.24	19.66	0.35	4.67	1.81	0.09	0.53	3.79
Nor1	20.16	1.29	0.44	2.11	9.39	0.00	0.00	1.56	0.00	0.43	0.99	2.59	0.29	0	0.26	2.07	1.44	0.05	-	-
Nor2	12.29	4.22	0.29	1.00	9.00	0.39	0.88	2.80	0.00	0.28	0.71	2.08	0.51	0	0.40	1.39	0.42	0.00	-	-
Sud1	12.97	3.89	0.00	0.93	4.96	0.80	0.21	1.40	0.00	0.34	1.31	1.62	0.00	0	0.12	2.26	0.43	0.81	-	-
WARDI	7.49	3.04	1.39	0.55	6.77	1.01	0.32	3.52	0.00	0.33	1.17	1.40	0.13	0	0.51	1.90	0.00	0.72	-	-
WARD4-1	22.68	-	-	2.38	3.61	1.53	0.66	0.77	0.00	0.67	0.82	3.40	0.29	0	0.38	1.47	1.24	0.46	1.54	4.15
WARD4-2	11.33	-	-	2.84	1.85	0.61	0.09	0.84	0.00	0.26	0.60	2.26	0.83	0	0.98	1.94	2.18	1.35	2.77	3.95

10.0 Bibliography

Abraitis, P. K., Pattrick, R. A. D., & Vaughan, D. J. 2004. Variations in the compositional, textural and electrical properties of natural pyrite: A review. *International Journal of Mineral Processing*, *74*1–4, 41–59. https://doi.org/10.1016/j.minpro.2003.09.002

Barbier, T., Berthebaud, D., Frésard, R., Lebedev, O. I., Guilmeau, E., Eyert, V., & Maignan, A. 2017. Structural and thermoelectric properties of n-type isocubanite $CuFe_2 S_3$. *Inorganic Chemistry Frontiers*, *4*3, 424–432. https://doi.org/10.1039/C6QI00510A

Barton, I. F., & Hiskey, J. B. 2022a. Chalcopyrite leaching in novel lixiviants. *Hydrometallurgy*, *207*, 105775. https://doi.org/10.1016/j.hydromet.2021.105775

Barton, I. F., & Hiskey, J. B. 2022b. Chemical, crystallographic, and electromagnetic variability in natural chalcopyrite and implications for leaching. *Minerals Engineering*, *189*, 107867. https://doi.org/10.1016/j.mineng.2022.107867

Barton, P. B. 1970. Sulfide Petrology. *Mineral Society of America*, *3*, 187–198. http://www.minsocam.org/MSA/OpenAccess_Publications/MSA_SP_3/MSA_SP3_187-198.pdf

Belousov, I., Danyushevsky, L., Goemann, K., Gilbert, S., Olin, P., Thompson, J., Lounejeva, E., & Garbe-Schönberg, D. 2023. STDGL3 , a Reference Material for Analysis of Sulfide Minerals by Laser Ablation ICP-MS: An Assessment of Matrix Effects and the Impact of Laser Wavelengths and Pulse Widths. *Geostandards and Geoanalytical Research*, *47*3, 493–508. https://doi.org/10.1111/ggr.12512

Berthebaud, D., Lebedev, O. I., & Maignan, A. 2015. Thermoelectric properties of n-type cobalt doped chalcopyrite Cu1−xCoxFeS2 and p-type eskebornite CuFeSe2. *Journal of Materiomics*, *1*1, 68–74. https://doi.org/10.1016/j.jmat.2015.03.007

Carr, W. D., & Morelli, D. T. 2016. The Thermoelectric Properties and Solubility Limit of CuFeS2(1−x)Se2x. *Journal of Electronic Materials*, *45*3, 1346–1350. https://doi.org/10.1007/s11664-015-4029-5

Crundwell, F. K. 2013. The dissolution and leaching of minerals. *Hydrometallurgy*, *139*, 132–148. https://doi.org/10.1016/j.hydromet.2013.08.003

Dreier, J. E. 2020. Management of Copper Heap Leach Projects: A Geologist's Perspective. *SEG Discovery*, *122*, 13–25. https://doi.org/10.5382/geo-and-mining-08

Drost, K., Chew, D., Petrus, J. A., Scholze, F., Woodhead, J. D., Schneider, J. W., & Harper, D. A. T. 2018. An Image Mapping Approach to U-Pb LA-ICP-MS Carbonate Dating and Applications to Direct Dating of Carbonate Sedimentation. *Geochemistry, Geophysics, Geosystems*, *19*12, 4631–4648. https://doi.org/10.1029/2018GC007850

Duran, C. J., Barnes, S.-J., Pleše, P., Kudrna Prašek, M., Zientek, M. L., & Pagé, P. 2017. Fractional crystallization-induced variations in sulfides from the Noril'sk-Talnakh mining district (polar Siberia, Russia). *Ore Geology Reviews*, *90*, 326–351. https://doi.org/10.1016/j.oregeorev.2017.05.016

Dutrizac, J. E. 1981. The dissolution of chalcopyrite in ferric sulfate and ferric chloride media. *Metallurgical Transactions B*, *12*2, 371–378. https://doi.org/10.1007/BF02654471

Dutrizac, J. E., & MacDonald, R. J. C. 1973. The synthesis of some copper sulfides and copper sulfosalts in 500–700 gram quantities. *Materials Research Bulletin*, *8*8, 961–971. https://doi.org/10.1016/0025-5408(73)90081-0

Eghbalnia, M. 2012. *ELECTROCHEMICAL AND RAMAN INVESTIGATION OF PYRITE AND CHALCOPYRITE OXIDATION*.

Fleet, M. E. 1970. Refinement of the crystal structure of cubanite and polymorphism of CuFeS2. *Zeitschrift Für Kristallographie - Crystalline Materials*, *132*1–6, 276–287. https://doi.org/10.1524/zkri.1970.132.16.276

Frenzel, N., & Frisch, G. 2022. Symmetry relationships between the crystal structures of chalcopyrite and its derivatives – a systematic approach to inform XRD analysis of Cu−Fe−S phases. *Zeitschrift Für Anorganische Und Allgemeine Chemie*, *648*10, e202200148. https://doi.org/10.1002/zaac.202200148

Ge, B., Shi, Z., Zhou, C., Hu, J., Liu, G., Xia, H., Xu, J., & Qiao, G. 2019. Enhanced thermoelectric performance of N-type eco-friendly material Cu1-xAgxFeS2 (x=0–0.14) via bandgap tuning. *Journal of Alloys and Compounds*, *809*, 151717. https://doi.org/10.1016/j.jallcom.2019.151717

George, L. L., Cook, N. J., Crowe, B. B. P., & Ciobanu, C. L. 2018. Trace elements in hydrothermal chalcopyrite. *Mineralogical Magazine*, *82*1, 59–88. https://doi.org/10.1180/minmag.2017.081.021

Gerischer, H. 1980. Photodecomposition of semiconductors thermodynamics, kinetics and application to solar cells. *Faraday Discussions of the Chemical Society*, *70*, 137. https://doi.org/10.1039/dc9807000137

Hankel, W. G. 1866. *Elektrische Untersuchungen: Über die thermoelektrischen Eigenschaften des Bergkrystalles* Vol. 7. Hirzel.

Hawley, J. E., & Nichol, I. 1961. Trace elements in pyrite, pyrrhotite and chalcopyrite of different ores. *Economic Geology*, *56*3, 467–487. https://doi.org/10.2113/gsecongeo.56.3.467

Hiskey, J. B. 1993. *Chalcopyrite Semiconductor Electrochemistry and Dissolution*.

Introduction to Hydrometallurgy. 2023.

Kwon, H., & Kim, I.-H. 2025. Effects of Ni Doping on Thermoelectric Properties of Chalcopyrite. *Materials*, *18*12, 2738. https://doi.org/10.3390/ma18122738

Lefèvre, R., Berthebaud, D., Mychinko, M. Yu., Lebedev, O. I., Mori, T., Gascoin, F., & Maignan, A. 2016. Thermoelectric properties of the chalcopyrite $Cu_{1-x}M_xFeS_{2-y}$ series (M = Mn, Co, Ni). *RSC Advances*, *6*60, 55117–55124. https://doi.org/10.1039/c6ra10046e

Li, J., Tan, Q., & Li, J.-F. 2013. Synthesis and property evaluation of CuFeS2−x as earth-abundant and environmentally-friendly thermoelectric materials. *Journal of Alloys and Compounds*, *551*, 143–149. https://doi.org/10.1016/j.jallcom.2012.09.067

Li, Y., Kawashima, N., Li, J., Chandra, A. P., & Gerson, A. R. 2013. A review of the structure, and fundamental mechanisms and kinetics of the leaching of chalcopyrite. *Advances in Colloid and Interface Science*, *197–198*, 1–32. https://doi.org/10.1016/j.cis.2013.03.004

Majuste, D., Ciminelli, V. S. T., Osseo-Asare, K., & Dantas, M. S. S. 2012. Quantitative assessment of the effect of pyrite inclusions on chalcopyrite electrochemistry under oxidizing conditions. *Hydrometallurgy*, *113–114*, 167–176. https://doi.org/10.1016/j.hydromet.2011.12.020

Mansur, E. T., Barnes, S.-J., & Duran, C. J. 2021. An overview of chalcophile element contents of pyrrhotite, pentlandite, chalcopyrite, and pyrite from magmatic Ni-Cu-PGE sulfide deposits. *Mineralium Deposita*, *56*1, 179–204. https://doi.org/10.1007/s00126-020-01014-3

McMillan, R. S., MacKinnon, D. J., & Dutrizac, J. E. 1982a. Anodic dissolution of n-type and p-type chalcopyrite. *Journal of Applied Electrochemistry*, *12*6, 743–757. https://doi.org/10.1007/BF00617495

McMillan, R. S., MacKinnon, D. J., & Dutrizac, J. E. 1982b. Anodic dissolution of n-type and p-type chalcopyrite. *Journal of Applied Electrochemistry*, *12*6, 743–757. https://doi.org/10.1007/BF00617495

Mindat.org. 2025, August 5. *Cu-Fe-S Mineral Search*. Cu-Fe-S Mineral Search. https://www.mindat.org/chemsearch.php?inc=Cu%2CFe%2CS%2C&exc=H%2CLi%2CBe%2CB%2CC%2CN%2CO%2CF%2CNa%2CMg%2CAl%2CSi%2CP%2CCl%2CK%2CCa%2CSc%2CTi%2CV%2CCr%2CMn%2CCo%2CNi%2CZn%2CGa%2CGe%2CAs%2CSe%2CBr%2CRb%2CSr%2CY%2CZr%2CNb%2CMo%2CRu%2CRh%2CPd%2CAg%2CCd%2CIn%2CSn%2CSb%2CTe%2CI%2CCs%2CBa%2CHf%2CTa%2CW%2CRe%2COs%2CIr%2CPt%2CAu%2CHg%2CTl%2CPb%2CBi%2CRa%2CREE%2CLa%2CCe%2CPr%2CNd%2CSm%2CEu%2CGd%2CTb%2CDy%2CHo%2CEr%2CTm%2CYb%2CLu%2CTh%2CU%2C&essential=0&class=0&sub=Search+Minerals

Murr, L. E., & Hiskey, J. B. 1981. Kinetic effects of particle-size and crystal dislocation density on the dichromate leaching of chalcopyrite. *Metallurgical Transactions B*, *12*2, 255–267. https://doi.org/10.1007/BF02654458

Nicol, M. J. 2022. Does galvanic coupling with pyrite increase the rate of dissolution of chalcopyrite under ambient conditions? An electrochemical study. *Hydrometallurgy*, *208*, 105824. https://doi.org/10.1016/j.hydromet.2022.105824

Norman, M. D., Pearson, N. J., Sharma, A., & Griffin, W. L. 1996. QUANTITATIVE ANALYSIS OF TRACE ELEMENTS IN GEOLOGICAL MATERIALS BY LASER ABLATION ICPMS: INSTRUMENTAL OPERATING CONDITIONS AND CALIBRATION VALUES OF NIST GLASSES. *Geostandards Newsletter*, *20*2, 247–261. https://doi.org/10.1111/j.1751-908X.1996.tb00186.x

O'Connor, G. M., & Eksteen, J. J. 2020. A critical review of the passivation and semiconductor mechanisms of chalcopyrite leaching. *Minerals Engineering*, *154*, 106401. https://doi.org/10.1016/j.mineng.2020.106401

Parker, A., Paul, R., & Power, G. 1981. Electrochemical aspects of leaching copper from chalcopyrite in ferric and cupric salt solutions. *Australian Journal of Chemistry*, *34*1, 13. https://doi.org/10.1071/CH9810013

Paul, B., Petrus, J., Savard, D., Woodhead, J., Hergt, J., Greig, A., Paton, C., & Rayner, P. 2023. Time resolved trace element calibration strategies for LA-ICP-MS. *Journal of Analytical Atomic Spectrometry*, *38*10, 1995–2006. https://doi.org/10.1039/d3ja00037k

Pridmore, D. F., & Shuey, R. T. 1976. The electrical resistivity of galena, pyrite, and chalcopyrite. *American Mineralogist*, *61*3–4, 248–259. https://pubs.geoscienceworld.org/msa/ammin/article-pdf/61/3-4/248/4203406/am61_248.pdf?casa_token=XJlo3vlZH4MAAAAA:M2AOkTmQ_af80SqQr5mAYcZdTt9omptaaMdUMRTnNVVfp_DEy2IF-xvQIy5EdtrWsaw_AL8

Ralph, J., Von Bargen, D., Martynov, P., Zhang, J., Que, X., Prabhu, A., Morrison, S., Li, W., Chen, W., & Ma, W. 2025. *Minerals that include Cu, Fe, S and exclude all other elements*. Mindat.Org. https://www.mindat.org/chemsearch.php?inc=Cu,Fe,S&eall=1

Ren, Z., Chao, C., Krishnamoorthy, P., Asselin, E., Dixon, D. G., & Mora, N. 2022. The overlooked mechanism of chalcopyrite passivation. *Acta Materialia*, *236*, 118111. https://doi.org/10.1016/j.actamat.2022.118111

Savard, D., Dare, S., Bédard, L. P., & Barnes, S. 2023. A New Mapping Protocol for Laser Ablation (with FAST-FUNNEL) Coupled to a TIME-OF-FLIGHT Mass Spectrometer (LA-FF-ICP-TOF-MS) for the

Rapid, Simultaneous Quantification of Multiple Minerals. *Geostandards and Geoanalytical Research*, *47*2, 243–265. https://doi.org/10.1111/ggr.12482

Shah, B. S., Chaki, S. H., Bhatt, S. V., & Deshpande, M. P. 2024. Flexible photodetector for broadband detection using wurtzite phase CuFeS2 nanoparticles. *Materials Science in Semiconductor Processing*, *179*, 108495. https://doi.org/10.1016/j.mssp.2024.108495

Shah, B. S., Chaki, S. H., & Deshpande, M. P. 2025. Synthesis, characterization and comparative thermoelectric behaviour study of two phases of CuFeS2 nanoparticles. *Next Materials*, *8*, 100549. https://doi.org/10.1016/j.nxmate.2025.100549

Singer, D. A. 2017. Future copper resources. *Ore Geology Reviews*, *86*, 271–279. https://doi.org/10.1016/j.oregeorev.2017.02.022

Tanne, C., & Schippers, A. 2021. Electrochemical investigation of microbially and galvanically leached chalcopyrite. *Hydrometallurgy*, *202*, 105603. https://doi.org/10.1016/j.hydromet.2021.105603

Telkes, M. 1950. Thermoelectric Power and Electrical Resistivity of Minerals. *MIT Solar Energy Conversion Research Project 26*, 536–555.

Teranishi, T., & Sato, K. 1975. OPTICAL, ELECTRICAL AND MAGNETIC PROPERTIES OF CHALCOPYRITE, $CuFeS_2$. *Le Journal de Physique Colloques*, *36*C3, C3-149-C3-153. https://doi.org/10.1051/jphyscol:1975327

Tippireddy, S., Azough, F., Bhui, A., Mikulska, I., Freer, R., Biswas, K., Vaqueiro, P., & Powell, A. V. 2023. Enhancement of thermoelectric properties of $CuFeS_2$ through formation of spinel-type microprecipitates. *Journal of Materials Chemistry A*, *11*42, 22960–22970. https://doi.org/10.1039/D3TA05011D

Tippireddy, S., Azough, F., Vikram, Tompkins, F. T., Bhui, A., Freer, R., Grau-Crespo, R., Biswas, K., Vaqueiro, P., & Powell, A. V. 2022. Tin-Substituted Chalcopyrite: An *n* -Type Sulfide with Enhanced Thermoelectric Performance. *Chemistry of Materials*, *34*13, 5860–5873. https://doi.org/10.1021/acs.chemmater.2c00637

Tsujii, N., & Mori, T. 2013. High Thermoelectric Power Factor in a Carrier-Doped Magnetic Semiconductor $CuFeS_2$. *Applied Physics Express*, *6*4, 043001. https://doi.org/10.7567/APEX.6.043001

Wilson, S. A., Ridley, W. I., & Koenig, A. E. 2002. Development of sulfide calibration standards for the laser ablation inductively-coupled plasma mass spectrometry technique. *J. Anal. At. Spectrom.*, *17*4, 406–409. https://doi.org/10.1039/B108787H

Xie, H., Su, X., Zheng, G., Yan, Y., Liu, W., Tang, H., Kanatzidis, M. G., Uher, C., & Tang, X. 2016. Nonmagnetic In Substituted $CuFe_{1-x}In_xS_2$ Solid Solution Thermoelectric. *The Journal of Physical Chemistry C*, *120*49, 27895–27902. https://doi.org/10.1021/acs.jpcc.6b10308

Xie, H., Su, X., Zheng, G., Zhu, T., Yin, K., Yan, Y., Uher, C., Kanatzidis, M. G., & Tang, X. 2017. The Role of Zn in Chalcopyrite $CuFeS_2$: Enhanced Thermoelectric Properties of $Cu_{1-x}Zn_xFeS_2$ with In Situ Nanoprecipitates. *Advanced Energy Materials*, *7*3, 1601299. https://doi.org/10.1002/aenm.201601299

Yevstigneyeva, T. L., Genkin, A. D., Troneva, N. V., Filimonova, A. A., & Tsepin, A. I. 1973. Shadlunite, a new sulfide of copper, iron, lead, manganese, and cadmium from copper nickel ores. *International Geology Review*, *15*11, 1341–1350. https://doi.org/10.1080/00206817309476022